Interference traps waves in open system: Bound states in the continuum

Almas F. Sadreev

Kirensky Institute of Physics, Federal Research Center KSC SB RAS, 660036 Krasnoyarsk, Russia

Abstract

I review the four mechanisms of bound states in the continuum (BICs) in application to microwave and acoustic cavities open to directional waveguides. The most simple are the symmetry protected BICs which are localized inside the cavity because of the orthogonality of the eigenmodes to the propagating modes of waveguides. However, the most general and interesting is the Friedrich-Wintgen mechanism when the BICs are result of full destructive interference of outgoing resonant modes. The third type of the BICs, the Fabry-Perot BICs, occur in a double resonator system when each resonator can serve as an ideal mirror. At last, the accidental BICs can be realized in the open cavities with no symmetry like the open Sinai billiard in which the eigenmode of the resonator can become orthogonal to the continuum of the waveguide accidentally by a smooth deformation of the eigenmode. We also review the one-dimensional systems in which the BICs occur owing to full destructive interference of two waves separated by spin or polarization or by paths in the Aharonov-Bohm rings. We widely use the method of effective non-Hermitian Hamiltonian equivalent to the coupled mode theory which detects bound states in the continuum (BICs) by finding zero widths resonances.

Keywords: Bound states in the continuum, Wave localization in one-dimensional wires, Open microwave and acoustic resonators, Effective non Hermitian Hamiltonian

Contents

1	Introduction	2
2	The effective non Hermitian Hamiltonian	4
3	Friedrich-Wintgen concept of BIC	5
4	Application to one-dimensional structures4.1Potential well4.2BICs in Aharonov-Bohm rings4.3Zeeman localization	8
5	BICs in two-dimensional planar open cavities	14
6	Accidental BICs in the Sinai shaped open cavity	20
7	The cylindrical resonator with non-axisymmetric waveguides. The twisted BICs. 7.1 Variation over the length of resonator at $\Delta \phi = \pi/4$	28

Email address: almas@tnp.krasn.ru (Almas F. Sadreev)

8	Spherical cavity			
	8.1 Two waveguides	38		
	8.2 Three waveguides	38		
9	The Fabry-Perot mechanism of BICs in the system of two coupled resonators	40		
10	Conclusions	43		

1. Introduction

More than two centuries has passed since Thomas Young presented his eminent double-slit experiment which unambiguously proved wave nature of light but still wave interference offers new phenomena in physics. Among the last ones to have attracted close attention of researches are bound states in the continuum (BICs). In 1929, von Neumann and Wigner [1] claimed that the single-particle Schrödinger equation could possess localized solutions that correspond to isolated discrete eigenvalues embedded in the continuum of positive energy states for some artificial oscillating bounded potential. Extension and some correction of this work was done by Stillinger and Herrick [2] who presented a few examples of spherically symmetric attractive local potentials with BICs of scattering states in the context of possible BICs in atoms and molecules (e.g., [3–6]). For a long time the phenomenon was considered as mathematical curiosity although physical mechanism is very similar to the mechanism of the Anderson localization. The BIC as a localized state is a result of precise destructive interference of waves scattered by the bounded potential in such a way that after enough distance we have no outgoing wave.

The decisive breakthrough came with paper by Friedrich and Wintgen [7] who formulated a general method to find BICs in quantum systems. The method based on the effective non-Hermitian Hamiltonian originates from Feshbach unified theory of nuclear reactions [8, 9] and uses the fact that the occurrence of BICs is directly related to the phenomenon of avoided level crossing. When two resonance states approach each other as a function of a certain continuous parameter, interference causes an avoided crossing of the two states in their energy positions and, for a certain value of the parameter, the width of one of the resonance states may vanish exactly. Since it remains above threshold for decay in to the continuum, this state becomes a BIC although each resonant state has a finite width. After numerous model considerations of different physical systems were presented [10–19].

The Fridrich-Wintgen (FW) approach of the effective Hamiltonian was first readily applied to planar metallic integrable billiard (cavity) open by attachment of two uniform plane waveguides [17] as shown in Fig. 1. The reader can find the descrip example, [20]). It was

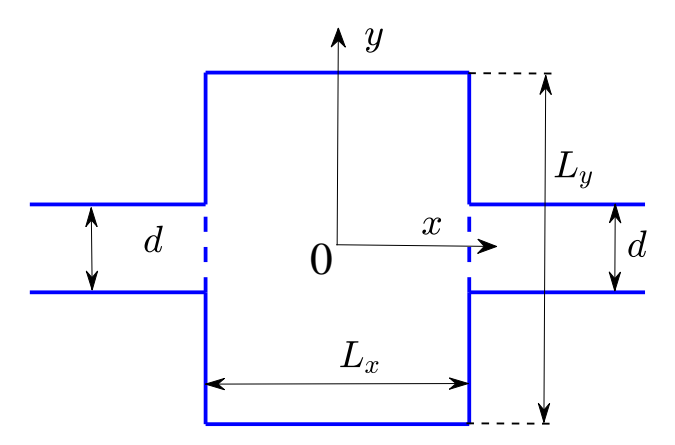


Figure 1: Two-dimensional plane resonator with two attached plane waveguides.

shown that for variation of resonator width W numerous events of degeneracy of the eigenmodes, say ψ_1 and ψ_2 occur. Then, at the points of degeneracy one can consider the superposed function $a\psi_1 + b\psi_2$. If each eigenmode is coupled with waveguide first channel by means W_1 and W_2 for the superposed function we have obviously the coupling $aW_1 + bW_2$ which can be tuned to zero by a proper choice of the superposition coefficients a and b. That

is an alternative interpretation of the BIC occurring at the degeneracy points in the integrable open resonators. The FW BICs were first experimentally observed by Lepetit and Kanté in metallic waveguide with two ceramic disks [21]. Similarly, Olendski and Mikhailovska have shown that in curved 2d waveguide a quasi-bound state formed as a result of the bend, at some critical parameters of the curve becomes a true bound state with in the continuum [22]. Catapan *et al* have revealed BICs in 2d straightforward stubbed quantum waveguide with impurities [23] and 2d serial structures [24]. Thus, it is turned out that going beyond 1d crucially increases opportunities for BICs.

The question of whether a wave can be perfectly confined (that is, whether a 'bound state' can exist) in an open system related to a simple frequency criterion. If the frequency of wave is outside the continuous spectral range spanned by the propagating waves, it can exist as a bound state because there is no pathway for it to radiate away. Conversely, a wave state with the frequency inside the continuous spectrum can only be a 'resonance' that leaks and radiates out to infinity. This is the conventional wisdom described in many books. A bound state in the continuum (BIC) is an exception to this conventional wisdom: it lies inside the continuum and coexists with extended waves, but it remains perfectly confined without any radiation.

Besides the Friedrich-Wintgen mechanism of full destructive interference other mechanisms for BICs exist. The most simple mechanism is the symmetry protection. Bolsterli has treated the special case in which there occur discrete states in the continuum in separable potentials [25]. In such a system a symmetry incompatibility decouples the square-integrable eigenmodes from the propagating modes of the waveguides [26–28]. It is accepted to determine such BICs as the symmetry protected ones. Less obvious but similar to the symmetry protected BICs are the accidental BICs when in spite of absence of symmetry arguments the coupling between the cavity eigenmode and the mode of the continuum can turn to zero accidentally by variation of the shape of the cavity as it was demonstrated in the open Sinai billiard [29]. Firstly, such a possibility was mentioned by Friedrich and Wintgen in the paper of physical realization of BICs in hydrogen atom in a magnetic field [30]. After accidental BICs were demonstrated in photonic systems [31, 32].

More sophisticated but transparent mechanism of BICs is the Fabry-Perot one. Assume, we have two ideal metallic mirrors parallel each other and separated by the distance L between them. All states are bounded in this system with eigenfrequencies $\omega_n = \pi n/L$, n = 1, 2, 3, ... If the mirrors have finite transmission probability all bound states become resonant states with finite line widths because of leakage through the mirrors [33]. Such a system is analogous to the simplest quantum mechanical problem of single particle in double barrier potential. In this one-dimensional system there are no BICs. However, in 1999 Kim and Satanin [34] put forward the idea to go beyond the one-dimensional case applying a temporally periodically driven barriers. Then, the effective dimensionality of the one-dimensional double barrier potential becomes two [35, 36] allowing for transmission zeros even for a finite height of the potential barriers. A possibility to localize quantum particle in a tight-binding chain with an off-channel impurity driven by an ac field was later considered by Longhi and Della Valle in a series of papers on Floquet BICs [37–39].

More straightforward Fabry-Perot models which supports BICs was considered by Shanhui Fan *et al* [40] in the framework of coupled mode theory [41]. In a series of papers [16, 42–44] two-dimensional identical quantum dots were used as Fabry-Perot mirrors. Then, the BICs are engineered by tuning the distance between the resonators coupled by wire. A similar approach was also used by Ordonez [45]. The same mechanism of BICs was exploited in photonic crystal systems [46–49]. The occurrence of BICs in these systems is accompanied by the collapse Fano resonances when transmission zero coalesces with the transmission unit [17, 21, 34]. Another variant of waveguide which supports BICs is double bend waveguide [50] due to transmission zeros in the bend [22].

Up to now we briefly discussed bound states with discrete frequencies embedded into the waveguide continua which are given by quantized due to a finite width of the waveguide (see Fig. 1). It is easy to realize the FW BIC embedded into the first continuum which is separated from the next continua by finite gap, say, by variation of length of resonator [17, 51–53] or obstacle size in the waveguide [24, 54]. The state of art is BICs embedded into a few continua of the waveguide [55]. At the first glance it seems impossible to support the BICs in the radiation continuum of free space which is given by continuous spectrum of light line (cone) $\omega = ck$ where c is the light velocity. The closed metallic resonator in free space is exceptional case because of its equivalence to quantum mechanical well potential with infinitely high walls. Similarly there might be the BICs in plasmonic nanostructures [56, 57]. It agrees with theorem that there are no BICs in the bounded domain which is complement of an unbounded domain [57, 58]. However, in infinite periodic arrays of dielectric particles light can leak only into a discrete number of diffraction orders allowing to find BICs embedded into a finite number of diffraction continua [59–61]. Therefore the infinite periodic dielectric structures can support BICs that attracts growing interest of the optical community because of

possibility to confine light. The extremely large quality factor of the BICs, or better to say, quasi-BICs and possibility to manipulate the BICs above light line has become of extreme importance in modern science and opens up many applications. In what follows we skip photonic BICs since they have already been a subject of recent reviews [62–65].

2. The effective non Hermitian Hamiltonian

One of the powerful and unambiguous means to diagnose BICs is the method of effective non Hermitian Hamiltonian [8, 66–70] which is equivalent to the coupled mode theory (CMT) [41, 71]. An important advantage of the effective non Hermitian Hamiltonian approach is a possibility to calculate the coupling matrix between closed system and continuum when the eigenmodes of subsystems are known [68, 72]. The approach of the effective non-Hermitian Hamiltonian [66, 67, 73] have found numerous applications in various branches of physics including atomic nuclei [69, 74], chaotic billiards [72, 75–79], tight-binding models [70, 80–83], potential scattering [69], photonic crystals [84], etc.

The objective of the present paper is to revisit the concept of the effective non-Hermitian Hamiltonian in application to open resonators with the Dirichlet or Neumann boundary conditions. The problem of resonant scattering typically involves a cavity (which could be quantum dot, microwave or acoustic cavity *etc*) and scattering channels coupled to the cavity. The mainstream idea is to split the full Hilbert space into subspaces: subspace *B* formed by the eigenfunctions of discrete spectrum localized within the scattering center, and subspaces *C* which spans the extended eigenfunctions of the scattering channels. Therefore, the exact description of open system meets a problem of matching the wave functions of discrete and continuous spectra. In 1958 Feshbach [8] introduced the idea to project the total Hilbert space onto the discrete states of subspace *B*. Given the Hamilton operator of the whole system as

$$\widehat{H} = \widehat{H}_B + \sum_{C} (\widehat{H}_C + \widehat{V}_{BC} + \widehat{V}_{CB}) \tag{1}$$

the projection onto the discrete subspace leads to the concept of the effective non-Hermitian Hamiltonian [8, 66–68]

$$\widehat{H}_{eff} = \widehat{\mathcal{H}}_B + \sum_C \widehat{V}_{BC} \frac{1}{E^+ - \widehat{H}_C} \widehat{V}_{CB}. \tag{2}$$

Here \widehat{H}_B is the Hamiltonian of the closed system, \widehat{H}_C is the Hamiltonian of the scattering channel C, \widehat{V}_{BC} , \widehat{V}_{CB} stand for the coupling matrix elements between the eigenstates of closed cavity and the eigenstates of the scattering channels, and E is the energy of scattered particle (wave). For EM wave or acoustic transmission $E = \omega^2$ where ω is the frequency. The term $E^+ = E + i0$ ensures that only outgoing waves will be present in the solution after the scattering occurs. As a result the effective Hamiltonian (2) is a non-Hermitian matrix with complex eigenvalues z_λ which determine the positions and lifetimes of the resonant states as $Re(z_\lambda)$, and $-2Im(z_\lambda)$ [66, 68]. If to assume that the propagation band of the continuum is not bounded then the effective non-Hermitian Hamiltonian takes the most simple form widely used in the scattering theory [67, 74, 77]

$$\widehat{H}_{eff} = \widehat{H}_B - i \sum_C \widehat{W}_C \widehat{W}_C^{\dagger}, \tag{3}$$

where \widehat{W}_C is a column matrix whose elements account for the coupling of each individual inner state to the scattering channel C. The scattering matrix $\mathcal{S}_{CC'}$ is then given by the inverse of $E - \widehat{H}_{eff}$ [67, 77]

$$\widehat{S} = \delta_{CC'} - 2i\widehat{W}^{+} \frac{1}{\widehat{H}_{eff} - E + i0} \widehat{W}, \tag{4}$$

where C = L, R. Therefore for the case of energy/frequency independent coupling matrix the complex eigenvalues coincide with the poles of the S-matrix.

However this formulation of the effective Hamiltonian is oversimplified because of unbounded spectrum of the continuum. Commonly the spectrum is bounded, at least below. For example, the electron has the spectrum $E = \frac{\hbar^2 k^2}{2m}$ and electromagnetic (EM) waves has the spectrum $\omega = ck$. Although the form for the effective Hamiltonian (3) is

preserved the coupling matrix elements become dependent on the energy or frequency [70–72]. In what follows we apply the method of the effective non Hermitian Hamiltonian to several physical systems: 1) One-dimensional wires with off-channel cavities the Aharonov-Bohm rings, 2) Two-dimensional microwave planar metallic waveguide consisted of the cavity and two attached waveguides and microelectronic waveguides (Fig. 1), and 3) Three-dimensional acoustic cylindrical and spherical resonators with attached cylindrical waveguides.

3. Friedrich-Wintgen concept of BIC

One can see that the effective non Hermitian Hamiltonian (3) consists of Hermitian part \widehat{H}_B whose eigenvalues are the eigenfrequencies of the closed cavity and the second anti-symmetric imaginary part. This part is a result of coupling of the cavity with the continua C of waveguides. The complex eigenvalues of the effective Hamiltonian have clear physical meaning. Their real parts respond for position of resonances while their imaginary parts respond for half resonant widths [66, 67]. Other words, if to prepare some field as the eigenmode of the closed cavity it will decay because of leakage of the mode into waveguides. Therefore the BIC is easily found out by turning to zero one of the imaginary parts of the complex eigenvalues of the non Hermitian effective Hamiltonian that was first established by Friedrich and Wintgen [7] in generic two-level Hamiltonian. When two resonance states approach each other as a function of a certain continuous parameter, interferences cause an avoided crossing of the two states in their energy positions and, for a certain value of the parameter, the width of one of the resonance states vanishes exactly. Since it remains above threshold for decay into the continuum, this state becomes a BIC. The Friedrich and Wintgen (FW) approach is significant by that it can be applicable to any waveguide system, in particular to microelectronic, microwave or acoustic resonators opened by attachment of waveguides [17, 80, 85].

Let the cavity undergoes degeneracy, for example, variation of shape. In the neighborhood of this degeneracy it is reasonable to truncate the Hamiltonian of the cavity by only those eigenvalues, say E_1 and E_2 , which are crossing. Moreover we assume that there is the only continuum with which the cavity modes are coupled. That gives the following two-level effective Hamiltonian

$$\widehat{H}_{eff} = \begin{pmatrix} \epsilon - i\gamma_1 & u - i\sqrt{\gamma_1\gamma_2} \\ u - i\sqrt{\gamma_1\gamma_2} & -\epsilon - i\gamma_2 \end{pmatrix}$$
 (5)

where without lose of generality we take $E_{1,2} = \pm \epsilon$. Also we introduce the $\gamma_1 = W_1^2$, $\gamma_2 = W_2^2$ which could define the resonant widths of the levels $E_{1,2}$ if the effective Hamiltonian (5) was diagonal. W_n , n = 1, 2 are the coupling constants of the cavity modes with waveguide propagating mode. Parameter u is responsible for repulsion of the eigenfrequencies of the closed cavity due to, for example, inner perturbation which removes the integrability of the cavity. For example, in Section 6 we consider a hole inside the cavity transforming into the Sinai billiard where the eigenlevels are avoided.

The advantage of the two-level approximation is that the BIC can be considered analytically [12, 17]. Let us write the transmission amplitude in the biorthogonal basis of the eigenstates of the effective non Hermitian Hamiltonian (5)

$$\widehat{H}_{eff}|\lambda\rangle = z_{\lambda}|\lambda\rangle, \ (\lambda|\lambda') = \delta_{\lambda,\lambda'}, \ |\lambda\rangle = |\lambda\rangle, \ (\lambda|=|\lambda\rangle^c = \langle\lambda|^*,$$
(6)

i,e., the left states are related to the right states via transposing. Then using the condition of completeness

$$\sum_{\lambda} |\lambda)(\lambda)| = 1$$

we can rewrite the transmission amplitude as sum of the resonant terms [70]

$$T = -2i \sum_{\lambda} \frac{V_{\lambda}^{L} V_{\lambda}^{R}}{E - z_{\lambda}} = -2i \sum_{\lambda} \frac{V_{\lambda}^{2}}{E - z_{\lambda}},$$
(7)

where $V_{\lambda}^{C} = V_{\lambda}$, C = L, R are the coupling constants of resonant states with the continuum or the propagating mode of waveguides. The expression (7) immediately shows us that the complex eigenvalues z_{λ} are the poles of the S-matrix provided that the matrix elements of the effective Hamiltonian are energy independent. Otherwise, we are to use the

complex scaling method [86] or to solve nonlinear fix point equations for real and imaginary parts of the complex eigenvalues z_{λ} which define the resonant positions and the resonant widths [68]. Relation of V_{λ} with the coupling constants W_n of the states of closed cavity with waveguides will be given below. Let us first consider the integrable resonator with u = 0 shown in Fig. 1. Then

$$z_{1,2} = -i\Gamma \pm \sqrt{(\epsilon - i\Delta\Gamma)^2 - \gamma_1 \gamma_2},\tag{8}$$

where

$$\Gamma = \frac{\gamma_1 + \gamma_2}{2}, \Delta\Gamma = \frac{\gamma_1 - \gamma_2}{2}.$$

For simplicity we take the coupling constants of the cavity eigenmodes with the propagating mode of waveguide equal $\gamma_1 = \gamma_2$. Such an simplification substantially shortens algebra of the eigenstates of the effective non Hermitian Hamiltonian. Then the right eigenstates are

$$|1) = \frac{1}{\sqrt{2\eta(\eta + i\epsilon)}} \begin{pmatrix} -\gamma \\ \eta + i\epsilon \end{pmatrix}, \quad |2) = \frac{1}{\sqrt{2\eta(\eta - i\epsilon)}} \begin{pmatrix} \gamma \\ \eta - i\epsilon \end{pmatrix}$$
 (9)

with corresponding eigenvalues

$$z_{1,2} = -i\gamma \pm \eta,\tag{10}$$

where $\eta = \sqrt{\gamma^2 - \epsilon^2}$. Let us write the following identity

$$\widehat{W} = \widehat{W} \sum_{\lambda} |\lambda\rangle\langle\lambda| = \sum_{\lambda} V_{\lambda}|\lambda\rangle \tag{11}$$

where V_{λ} are the coupling constants between the resonant states and the continuum. Therefore from Eq. (9) we obtain the link between coupling constants W_n where n enumerates the closed resonator states and V_{λ} where λ enumerates the resonant states:

$$V_1 = \frac{W}{\sqrt{2\eta(\eta + i\epsilon)}} (\eta + i\epsilon - \gamma), \quad V_2 = \frac{W}{\sqrt{2\eta(\eta - i\epsilon)}} (\eta - i\epsilon + \gamma)$$
 (12)

where $W = W_1 = W_2$.

The BIC occurs when $\epsilon = 0$. The eigenstates limit to

$$|1\rangle = \frac{1}{\sqrt{2}} \begin{pmatrix} -1\\1 \end{pmatrix}, \quad |2\rangle = \frac{1}{\sqrt{2}} \begin{pmatrix} 1\\1 \end{pmatrix}. \tag{13}$$

From Eq. (12) one can see that the resonant state |1) decouples from the continuum at $\epsilon=0$ while the state |2) acquires maximal coupling with the continuum (superradiant state). Therefore the state |1) can be qualified as the FW BIC decoupled from the continuum owing to exact destructive interference of leaking eigenmodes of the closed cavity |1⟩ and |2⟩. For such a simplified case of equal coupling constants and u=0 we see the difference between the FW BIC which has $V_1(\epsilon=0)=0$ in respect to the eigenstates | λ ⟩ of \widehat{H}_{eff} and the symmetry protected BIC which has $W_1=0$ in respect to the eigenstate of \widehat{H}_B of the closed cavity. General case of N levels was considered in Ref. [87] where it is proved that decoupling from all channels of the continuum described is a necessary and sufficient condition for a resonance state to be the BIC, i.e., the state with vanishing decay width.

The transmittance is plotted in Fig. 2 (a) which demonstrates that at the BIC point E=0, $\epsilon=0$ the maximal transmittance coalesces with the maximal reflectance (collapse of Fano resonance [34]). Simultaneously at the BIC point we observe in Fig. 2 (b) that the resonant width turns to zero.

Let consider the transmittance in the vicinity of the BIC's point $\epsilon = 0$, E = 0. The eigenvalues of \widehat{H}_{eff} can be approximated as $z_1 \approx -i\epsilon^2/2\Gamma$, $z_2 \approx -2i\Gamma$. Then the transmission amplitude (7) takes the simple form

$$T(E,\epsilon) \approx -\frac{2iE\Gamma}{2E\Gamma + i\epsilon^2}.$$
 (14)

It follows |T| = 0 for E = 0, $\epsilon \neq 0$, and |T| = 1 for $\epsilon = 0$, $E \neq 0$. Therefore, the BIC is a singular point in the sense that the value of the transmission amplitude depends on the way to approach this point. If $\Delta\Gamma \neq 0$ the transmission

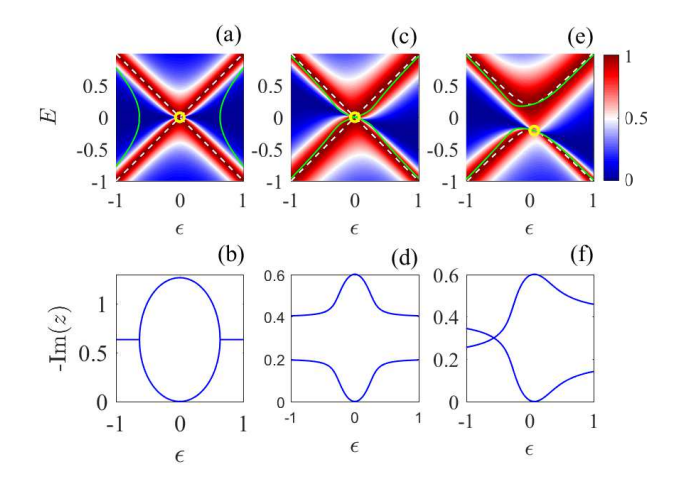


Figure 2: The transmittance, eigenlevels of closed system (dash white lines), resonant positions (solid green lines), resonant widths (solid lines, below) and BICs (open circles) in two-level description of the effective Hamiltonian (5). (a) and (b) $\gamma_1 = \gamma_2 = 0.1$, u = 0; (c) and (d) $\gamma_1 = 0.1$, $\gamma_2 = 0.2$, u = 0; (e) and (f) $\gamma_1 = 0.1$, $\gamma_2 = 0.2$, u = 0.5.

zero follows $E = \epsilon \Delta \Gamma / \Gamma$. In general case of different coupling constants γ_1 , γ_2 and $u \neq 0$ we will follow Kikkawa *et al* [88]. We have for the eigenvalues of the effective Hamiltonian (5)

$$(z + \epsilon + i\gamma_1)(z - \epsilon + i\gamma_2) - (u - i\sqrt{\gamma_1\gamma_2})^2 = 0.$$
(15)

Then we have for the roots of this equation according to the Vietta's formula

$$z_1 + z_2 = -i(\gamma_1 + \gamma_2),$$

$$z_1 z_2 = -(\epsilon + i\gamma_1)(\epsilon - i\gamma_2) - (u - i\sqrt{\gamma_1\gamma_2})^2 = -\epsilon^2 - u^2 + 2i(u\sqrt{\gamma_1\gamma_2} - \epsilon(\gamma_1 - \gamma_2)).$$
(16)

At the BIC's point one of the roots, say z_1 , is real. In that case, the roots can be expressed using real quantities A and B as

$$z_1 = A,$$

 $z_2 = B - i(\gamma_1 + \gamma_2).$ (17)

Substitution of Eq. (17) into Eq. (16) gives

$$A + B = 0,$$

$$AB = -\epsilon^2 - u^2.$$
 (18)

On the other hand, by comparing the imaginary parts of both sides of Eq. (16) after substitution we obtain

$$A = -\frac{\epsilon(\gamma_1 - \gamma_2) + 2u\sqrt{\gamma_1\gamma_2}}{\gamma_1 + \gamma_2}.$$
 (19)

Finally from Eqs. (18) and (19) we obtain the following equation for the BIC's point

$$u(\gamma_1 - \gamma_2) = 2\epsilon \sqrt{\gamma_1 \gamma_2}. (20)$$

First, this equation for the BIC point in two-level approximation was obtained by Volya and Zelevinsky [12], and solution is shown in Fig. 2 (e) and (f).

4. Application to one-dimensional structures

4.1. Potential well

Let us consider the textbook problem of quantum particle propagation in one-dimensional potential relief like shown in Figure 1 in a review by Hsu *et al* [62]. The wave functions in the segments of the structure are the follows

$$\psi_L(x) = \exp(ikx) + r \exp(-ikx),$$

$$\psi(x) = a \exp(iqx) + b \exp(-iqx),$$

$$\psi_R(x) = t \exp(ikx).$$
(21)

By use of the boundary conditions we can write the following equation for the solution

$$\hat{L}\vec{\psi} = \vec{g},\tag{22}$$

where $\hat{L}(k)$ is the following matrix

$$\begin{pmatrix} -1 & 1 & 1 & 0 \\ k & q & -q & 0 \\ 0 & e^{iqL} & e^{-iqL} & -e^{ikL} \\ 0 & qe^{iqL} & -qe^{-iqL} & -0e^{ikL} \end{pmatrix},$$
(23)

 $\vec{g}^T = (1 \ k \ 0 \ 0), \ \vec{\psi}^T = (r \ a \ b \ t), \text{ and } L \text{ is the width of the potential well. The determinant of matrix } \hat{L}(k) \text{ equals:}$

$$2i(k^2 + q^2)\sin(kL) + 4kq\cos(kL) \tag{24}$$

is the denominator of the S-matrix [89] zeros of which define its poles. The BIC is the solution of the inhomogeneous part of Eq. (22) when $\vec{g} = 0$. In order there were a BIC the determinant (24) is to be turn to zero that can not be fulfill for that case of one-dimensional potential well. Therefore the one-dimensional potential can not support localized states with energy embedded into the continuum of extended states with E > 0. This is the conventional wisdom described in many books. A bound state in the continuum (BIC) is an exception to this conventional wisdom: it lies inside the continuum and coexists with extended waves, but it remains perfectly confined without any leakage. In 1929, von Neumann and Wigner [1] discovered that the long-range oscillating attractive one-dimensional potential can support BICs. The BIC is a classical paradox of a quantum particle with the energy enough to leak from the potential well and nevertheless remaining spatially confined. The Neumann-Wigner BIC emerges due to precise destructive interference of waves scattered by a bound potential in such a way that, after enough distance, we obtain localized state. The physics of localization is similar to Anderson localization in random potential [90]. For a long time the phenomenon was considered as mathematical curiosity because hardly such potentials invented by von Neumann and Wigner (corrections of the potentials were done by Stillinger [2]) can be realized experimentally.

4.2. BICs in Aharonov-Bohm rings

The Aharonov-Bohm oscillations of conductance are another bright example of wave interference when electron encircling upper or down arms of ring acquires additional magnetic flux phases $\pm \gamma/2$ where $\gamma = 2\pi\Phi/\Phi_0$, $\Phi = B\pi R^2$ is the magnetic flux, $\Phi_0 = 2\pi\hbar c/e$ [91]. In this subsection we show that particular case of full destructive interference gives rise to localization of electron inside the ring, i.e., BICs [92].

Following Xia [93] we write the wave functions in the segments of the structure shown in Fig. 3 (a) as

$$\psi_{1}(x) = \exp(ikx) + r \exp(-ikx),
\psi_{2}(x) = a_{1} \exp(ik^{-}x) + a_{2} \exp(-ik^{+}x),
\psi_{3}(x) = b_{1} \exp(ik^{+}x) + b_{2} \exp(-ik^{-}x),
\psi_{4}(x) = t \exp(ikx),$$
(25)

where $k^- = k - \gamma$, $k^+ = k + \gamma$. All variables are dimensionless via the ring length $2\pi R$. The boundary conditions (the continuity of the wave functions and the conservation of the current density) allow to find all coefficients in (25). We write the corresponding equation in matrix form

$$\hat{F}\vec{\psi} = \vec{g},\tag{26}$$

where $\hat{F}(k, \gamma)$ is the following matrix

$$\begin{pmatrix}
-1 & 0 & 1 & 1 & 0 & 0 \\
-1 & 0 & 0 & 0 & 1 & 1 \\
0 & -1 & e^{ik^{-}/2} & e^{-ik^{+}/2} & 0 & 0 \\
0 & -1 & 0 & 0 & e^{ik^{+}/2} & e^{-ik^{-}/2} \\
1 & 0 & \frac{k^{-}}{k} & -\frac{k^{+}}{k} & \frac{k^{+}}{k} & -\frac{k^{-}}{k} \\
0 & -1 & \frac{k^{-}}{k}e^{i\frac{k^{-}}{2}} & -\frac{k^{+}}{k}e^{-i\frac{k^{+}}{2}} & \frac{k^{+}}{k}e^{i\frac{k^{+}}{2}} & -\frac{k^{-}}{k}e^{-i\frac{k^{-}}{2}}
\end{pmatrix},$$
(27)

 $\vec{g}^T = (1\ 1\ 0\ 0\ 1\ 0)$. The vector $\vec{\psi}^T = (r\ t\ a_1\ a_2\ b_1\ b_2)$ is the solution for the scattering wave function:

$$r = 2(3\cos k - 4\cos \gamma + 1)/Z,$$

$$t = 16i(\sin \frac{k}{2}\cos \frac{\gamma}{2})/Z$$

$$a_1 = 2(2e^{i\gamma} - 3e^{-ik} + 1)/Z,$$

$$a_2 = 2(e^{ik} + 1 - 2e^{i\gamma})/Z,$$

$$Z = 8\cos \gamma - 9e^{-ik} - e^{ik} + 2,$$
(28)

 $b_{1,2}(k,\gamma) = a_{1,2}(k,-\gamma)$. In Fig. 3 we show lines of the transmission zeros ($|t(k,\gamma)| = 0$, dashed lines) which cross the lines of the transmission ones ($|t(k,\gamma)| = 1$, solid lines) at points

$$k_m = 2\pi m, m = \pm 1, \pm 2, ...,$$

 $\gamma_n = 2\pi n, n = 0, \pm 1, \pm 2,$ (29)

As can be seen from the expression for the denominator Z in Eq. (28), the imaginary part of the poles vanishes at

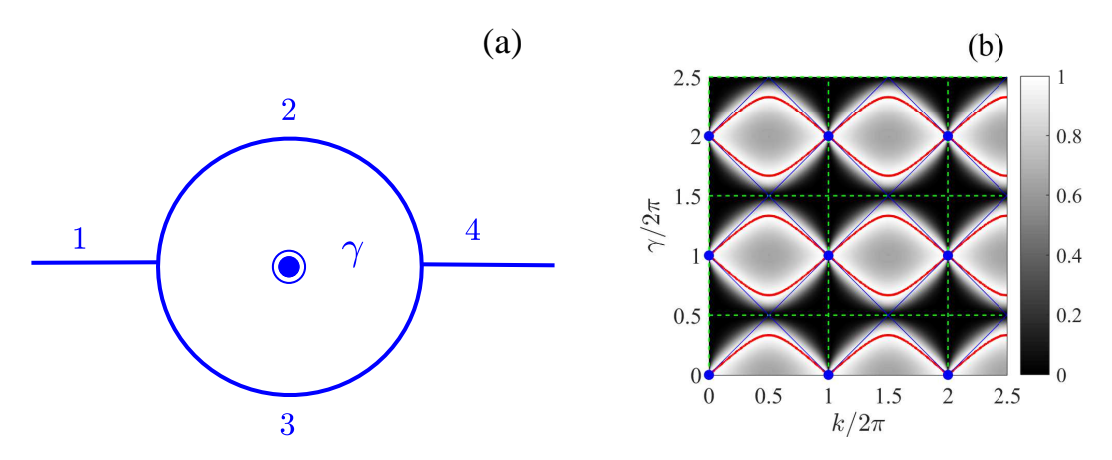


Figure 3: (a) One-dimensional ring thread by the magnetic flux γ and opened by attachment of two leads. (b) Transmission through the ring vs the magnetic flux and wave number $k = \sqrt{E}$. Green dash lines show transmission zeros $|t|^2 = 0$ and solid red lines show transmission ones $|t|^2 = 1$. The BICs are marked by blue closed circles. Blue thin solid lines show wave numbers as dependent on the flux $k = (m - \gamma)$ where m are integers.

these points. Simultaneously, a degeneracy of eigen energies of closed ring $(k_m - \gamma)^2$ occurs at these points. Here m is the azimuthal index (magnetic quantum number) that defines the eigenfunctions of the closed ring $\psi_m(x) = \exp(ik_m x)$. The point k = 0 is excluded from the consideration since it gives zero conductance. An existence of the peculiar points (29) were shown in Ref. [14] as a points where the density of states shows similar collapses as collapses of the Fano resonance in the transmission. To show that the BICs appear at the points (29), let us consider one of the points, say, $\mathbf{s}_0 = (k_1, \gamma_1) = 2\pi(1, 1)$. All the other points are equivalent because of the periodical dependence of the system on k and γ . In the vicinity of the point \mathbf{s}_0 we write Eq. (28) in the following approximated form

$$t \approx \frac{\Delta k}{\Delta k + i(\Delta \gamma)^2 / 2}, \quad r \approx \frac{i(3\Delta k^2 - 4\Delta \gamma^2)}{4(2\Delta k + i\Delta \gamma^2)},$$

$$a_1 \approx \frac{3\Delta k + 2\Delta \gamma}{4\Delta k + 2i\Delta \gamma^2}, \quad a_2 \approx \frac{\Delta k - 2\Delta \gamma}{4\Delta k + 2i\Delta \gamma^2},$$
(30)

where $\Delta k = k - k_1$, $\Delta \gamma = \gamma - \gamma_1$. The transmission amplitude in the vicinity of the BIC point \mathbf{s}_0 in (30) is similar to the expressions obtained for a shifted von Neumann-Wigner potential [4] or two-level approximated approach (see Eq. (14)). One can see that all amplitudes $a_{1,2}$, $b_{1,2}$ of the inner wave functions are singular at the point \mathbf{s}_0 . Such a result for the BIC points was firstly found by Pursey and Weber [4]. At this point the matrix (27) takes the following form

$$\hat{F}(\mathbf{s}_0) = \begin{pmatrix} -1 & 0 & 1 & 1 & 0 & 0 \\ -1 & 0 & 0 & 0 & 1 & 1 \\ 0 & -1 & 1 & 1 & 0 & 0 \\ 0 & -1 & 0 & 0 & 1 & 1 \\ 1 & 0 & 0 & -2 & 2 & 0 \\ 0 & -1 & 0 & -2 & 2 & 0 \end{pmatrix}. \tag{31}$$

The determinant of the matrix $\hat{F}(\mathbf{s}_0)$ equals zero. Therefore, $\hat{F}\vec{f}_0=0$. By direct substitution of the vector $\vec{f}_0^T=\frac{1}{2}(0\ 0\ 1\ -1\ -1\ 1)$ one can verify that \vec{f}_0 is the right eigenvector which is the null vector. The corresponding left null eigenvector is $\tilde{f}_0 = \frac{1}{2}(-1\ 1\ 1\ -1\ 0\ 0)$. It is well known from linear algebra, that if the determinant of matrix \hat{F} is equaled to zero, then the necessary and sufficient condition for existence of solution of the equation (26) is that the vector \tilde{f}_0 is orthogonal to vector \vec{g} [94]. In holds, indeed, $\tilde{f}_0 \cdot \vec{g} = 0$. Therefore, the null vector \tilde{f}_0 is proven to be the BIC. The general solution of Eq. (26) at the point \mathbf{s}_0 can therefore be presented as

$$\vec{\psi}(\mathbf{s}_0) = \alpha \vec{f_0} + \vec{\psi_p},\tag{32}$$

where α is an arbitrary coefficient and ψ_p^T is particular transport solution of Eq. (26). By direct substitution one can verify that $\psi_p^T = \left(0.1.\frac{3}{4}.\frac{1}{4}.\frac{3}{4}.\frac{1}{4}\right)$ is the particular solution of Eq. (26). It is worthwhile to note that this result completely agrees with the scattering theory on graphs [95, 96]. Texier has shown that for certain graphs the stationary scattering state gives the solution of the Schrödinger equation for the continuum spectrum apart for discrete set of energies where some additional states are localized in the graph and thus are not probing by scattering, leading to the failure of the state counting method from the scattering.

4.3. Zeeman localization

Although open the Aharonov-Bohm ring consists of 1d wires, the ring is two-dimensional in order electron could encircle the flux. In this subsection we present the model which is indeed one-dimensional but capable to localize electron. We go beyond the scalar Helmhotz equation and employ the interference of spin polarized resonant states of the one-dimensional electron transmission [97]. Let us consider three domains in which external stationary magnetic field is applied as sketched in Fig. 4. Assume the external magnetic field \vec{B} inside the central layer is tilted relative to the outer magnetic field oriented along z-axis. We also assume that the inner layer has the potential shifted relative to the outer layers by a value U_0 . Outside of the central layer electron has two split energy spectra $E = k_{\sigma}^2 \mp B$, $\sigma = \uparrow, \downarrow$ which specify the continua by the wave vector \vec{k}_{σ} . In the central layer the spin dependent spectra have the following form $E = q_s^2 + U_0 \mp B$, s = 1, 2 which specify spin dependent channels by the vector \vec{q}_s . Owing to choice of the potential step $(U_0 = -20)$ as depicted in Fig. 4 by green both spin channels are open in the central layer while outside only the spin up continuum is open for E < B. Therefore only the electron with spin up participates in electron transmission and reflection.

Let us write the Schrödinger equation for the toy model of electron in magnetic field (see Fig. 4):

$$\left[\frac{1}{2m}(i\hbar\nabla + \frac{e}{c}\mathbf{A})^2 + U_0(z) - \sigma\mathbf{B}(z) - E\right]\Psi = 0.$$
(33)

The orbital motion has characteristic length $a_B^2 = \frac{\hbar c}{eB}$ which in the magnetic field of $10^3 Oe$ equals 100 nm. Then for layer of thickness $L \ll a_B$ we can disregard the orbital contribution in Eq. (33) and rewrite as follows

$$\left[\nabla^2 - U_0(z) + \sigma \mathbf{B}(z) + E\right] \Psi = 0. \tag{34}$$

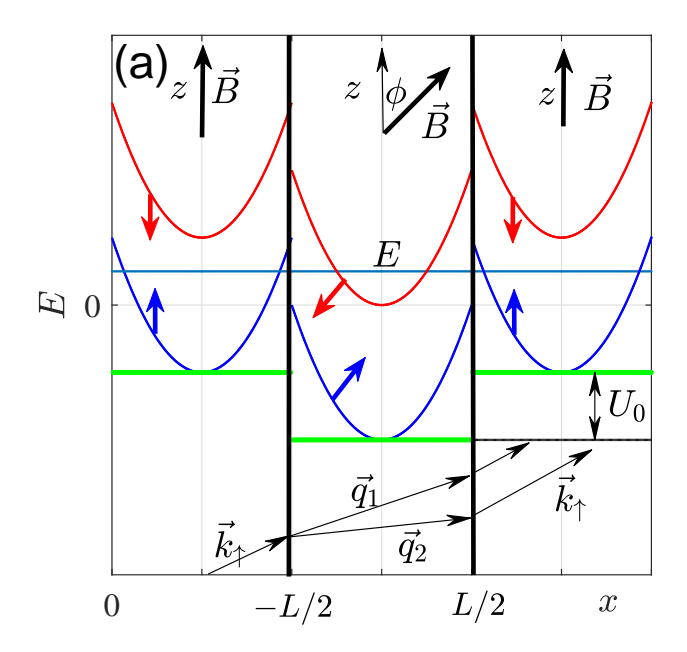


Figure 4: An one-dimensional spin model for illustration of BICs due to full destructive interference of spin polarized resonant states. Beyond the central layer, the magnetic field \vec{B} is directed along the z-axis, inside the central layer \vec{B} is tilted by angle ϕ . The spin-up electron falls by angle θ with the energy below the spectrum of spin-down and splits into two states specified by \vec{k}_1 and \vec{k}_2 .

Next we substitute the step-wise magnetic filed as shown in Fig. 4. Then Hamiltonian (34) will take the following form

$$\widehat{H} = \begin{cases} -\frac{d^2}{dz^2} - \sigma_x B & \text{if } |z| > L/2; \\ -\frac{d^2}{dz^2} + U_0 - \sigma_x B \cos(\phi) - \sigma_z B \sin(\phi) & \text{if } |z| < L/2. \end{cases}$$
(35)

In the outer layers which form the radiation continua with the following propagating solutions

$$\Psi_{\vec{k}}(\vec{x}) = \exp(i\vec{k}_{\sigma}\vec{x})|\sigma\rangle,\tag{36}$$

where $\sigma = \uparrow, \downarrow$,

$$|\uparrow\rangle = \begin{pmatrix} 1\\0 \end{pmatrix}, |\downarrow\rangle = \begin{pmatrix} 0\\1 \end{pmatrix}, \tag{37}$$

and

$$E = k_{\sigma}^2 \mp B. \tag{38}$$

Respectively for the inner layer we have

$$\Psi_{\vec{q}_s}(\vec{x}) = \exp(i\vec{q}_s\vec{x})|s\rangle,\tag{39}$$

where s = 1, 2,

$$|1\rangle = \begin{pmatrix} \cos(\phi/2) \\ \sin(\phi/2) \end{pmatrix}, |2\rangle = \begin{pmatrix} -\sin(\phi/2) \\ \cos(\phi/2) \end{pmatrix},$$
 (40)

and

$$E = q_s^2 + U_0 \mp B. \tag{41}$$

Let us choose the energy of incident electron that only spin up channel is open. Then at the left (z < -L/2) we have

$$\Psi_L(\vec{x}) = (e^{i\vec{k}_\uparrow \vec{x}} + r_\uparrow e^{-i\vec{k}_\uparrow \vec{x}})|\uparrow\rangle. \tag{42}$$

Inside the defect layer (|z| < L/2) both channels are open due to proper choice of the potential $U_0 = -20$ and therefore one can present the solutions as follows

$$\Psi_B(\vec{x}) = \sum_{s=1,2} (a_s e^{i\vec{q}_s \vec{x}} + b_s e^{-i\vec{q}_s \vec{x}}) |s\rangle. \tag{43}$$

At last at the right side (z > L/2) we write

$$\Psi_R(\vec{x}) = t_{\uparrow} e^{i\vec{k}_{\uparrow} \cdot \vec{x}} |\uparrow\rangle. \tag{44}$$

Here r_{\uparrow} and t_{\uparrow} are the reflection and transmission amplitudes. Next, assume electron with spin σ incidents with wave vector $\vec{k}_{\sigma} = (k_{x\sigma}, k_{z\sigma})$ and reflecting with the reflection amplitude r_{σ} . Because of preservation of transverse component of moment $k_{x\sigma} = k_{xs} = k_x$ we obtain the following equations:

$$1 + r_{\uparrow} = (a_{1} + b_{1})\cos(\phi/2) - (a_{2} + b_{2})\sin(\phi/2),$$

$$k_{z\uparrow}(1 - r_{\uparrow}) = q_{z1}(a_{1} - b_{1})\cos(\phi/2) - q_{z2}(a_{2} - b_{2})\sin(\phi/2),$$

$$r_{\downarrow} = (a_{1} + b_{1})\sin(\phi/2) + (a_{2} + b_{2})\cos(\phi/2),$$

$$-k_{z\downarrow}r_{\downarrow} = q_{z1}(a_{1} - b_{1})\sin(\phi/2) + q_{z2}(a_{2} - b_{2})\cos(\phi/2),$$

$$t_{\uparrow}e^{ik_{z\uparrow}L} = (a_{1}e^{iq_{z1}L} + b_{1}e^{-iq_{z1}L})\cos(\phi/2) - (a_{2}e^{iq_{z2}L} + b_{2}e^{-iq_{z2}L})\sin(\phi/2),$$

$$k_{z\uparrow}t_{\uparrow}e^{ik_{z\uparrow}L} = q_{z1}(a_{1}e^{iq_{z1}L} - b_{1}e^{-iq_{z1}L})\cos(\phi/2) - q_{z2}(a_{2}e^{iq_{z2}L} - b_{2}e^{-iq_{z2}L})\sin(\phi/2),$$

$$t_{\downarrow}e^{ik_{z\downarrow}L} = (a_{1}e^{iq_{z1}L} + b_{1}e^{-iq_{z1}L})\sin(\phi/2) + (a_{2}e^{iq_{z2}L} + b_{2}e^{-iq_{z2}L})\cos(\phi/2),$$

$$k_{z\downarrow}t_{\downarrow}e^{ik_{z\downarrow}L} = q_{z1}(a_{1}e^{iq_{z1}L} - b_{1}e^{-iq_{z1}L})\sin(\phi/2) + (a_{2}e^{iq_{z2}L} - b_{2}e^{-iq_{z2}L})\cos(\phi/2).$$

$$(45)$$

The transmission probability versus the thickness of potential well L and incident energy or angle of incidence θ is plotted in Fig. 5 (a) and (b) respectively where one can see typical points for BICs with collapse of Fano resonance is observed. These points unambiguously indicate the BIC points. Indeed, the BIC as localized mode inside the layer can

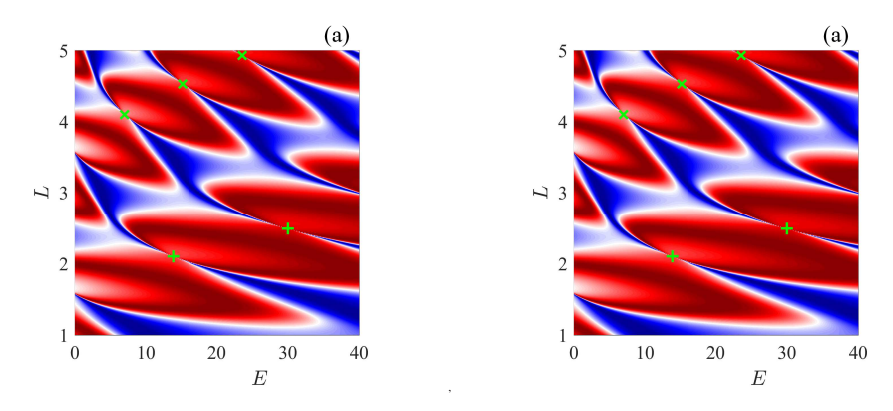


Figure 5: Reflection probability of the spin-up electron for B=10 tilted by angle $\phi=\pi/3$ and $U_0=-20$ vs (a) incident energy E and central layer thickness E at angle of incidence $\theta=\pi/4$, and (b) vs angle of incidence θ and central layer thickness E at incident energy E=30 and $\phi=\pi/4$. Magenta pluses mark the points of the BICs symmetric with respect to the center of the layer, while crosses mark the points of antisymmetric BICs.

be found from equations of continuity at the interfaces. These equations can be simplified with account of symmetry relative to $z \rightarrow -z$. Then the symmetric BIC can be written as

$$\psi_{BIC,sym}(z) = \begin{cases} a\cos(q_{z1}z)|1\rangle + b\cos(q_{z2}z)|2\rangle & \text{if } |z| < L/2\\ ce^{(-|k_{z1}|z)}|\downarrow\rangle & \text{if } |z| > L/2. \end{cases}$$
(46)

where the last contribution is the result of evanescent mode with spin down and asymmetric BIC

$$\psi_{BIC,asym}(z) = \begin{cases} a \sin(q_{z1}z)|1\rangle + b \sin(q_{z2}z)|2\rangle & \text{if } |z| < L/2\\ sign(z)ce^{(-|k_{z1}|z)|} \downarrow \rangle & \text{if } |z| > L/2. \end{cases}$$
(47)

Table 1: Quantum/Optical correspondence.

, , , , , , , , , , , , , , , , , , , ,					
Quantum mechanics	Optics				
electron	photon				
$\psi, \frac{\partial \psi}{\partial z}$	E , B				
spin	polarization				
energy	frequency				
$ \downarrow\rangle$	TE-wave				
$ \uparrow\rangle$	TM-wave				
magnetic field	anisotropy axis				

We imply that the modes equal zero at the spin up continuum and obey the continuity equations for the evanescent mode spin down. As the result we obtain the following equations for the symmetric BIC

$$a\cos(\phi/2)\cos(q_{z1}L/2) - b\sin(\phi/2)\cos(q_{z2}L/2) = 0,$$

$$a\sin(\phi/2)\cos(q_{z1}L/2) + b\cos(\phi/2)\cos(q_{z2}L/2) = ce^{(-|k_{z\downarrow}|L/2)},$$

$$aq_{z1}\sin(\phi/2)\sin(q_{z1}L/2) + bq_{z2}\cos(\phi/2)\sin(k_{z2}L/2) = c|k_{z\downarrow}|e^{(-|k_{z\downarrow}|L/2)}.$$
(48)

Thus, we obtain the following equation for the symmetric BIC points

$$-\tan^{2}(\phi/2) = \frac{q_{z2}\tan(q_{z2}L/2) - |q_{z\downarrow}|}{k_{z1}\tan(q_{z1}L/2) - |k_{z\downarrow}|},$$
(49)

and respectively for the asymmetric BIC points

$$-\tan^2(\phi/2) = \frac{q_{z2}\cot(q_{z2}L/2) + |k_{z\downarrow}|}{q_{z1}\cot(q_{z1}L/2) + |k_{z\downarrow}|}.$$
 (50)

The solutions of Eqs. (48) and (49) are marked in Fig. 5 by pluses and crosses respectively which exactly coincide with points of Fano resonance collarse. The lowest symmetric and antisymmetric BIC solutions are shown in Fig. 6.

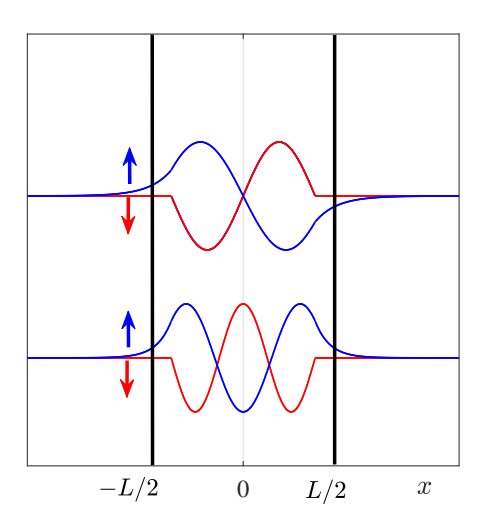


Figure 6: The BIC solutions, symmetric and antisymmetric, in the layered structure.

In Table 1 we establish the one-by-one correspondence between the spin of the electron and the polarization state of light. Owing that these BICs were verified experimentally by full destructive interference of light paths with TM and TE polarizations in anisotropic layer [97].

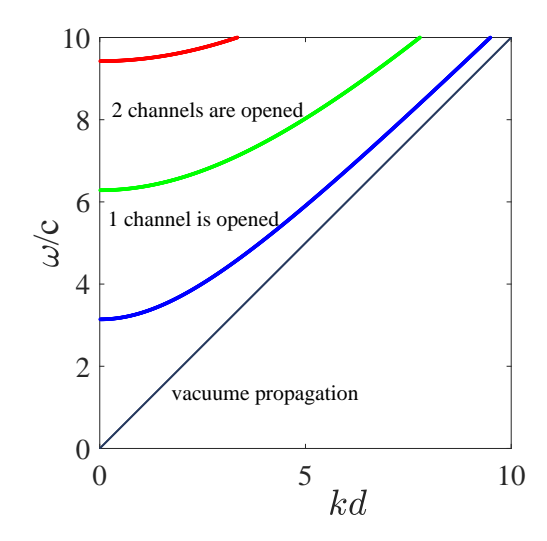


Figure 7: Dispersion curves of open channels in planar waveguide with rectangular cross-section.

5. BICs in two-dimensional planar open cavities

Two- and three-dimensional wave transmission through cavities is distinct of one-dimensional transmission. First, by change of shape of the 2d or 3d cavity we can achieve a degeneracy in 1d resonator and therefore avoided crossing of resonances. Second, 2d and 3d waveguides attached to the 2d and 3d cavities can support finite number of open channels as dependent on wave frequency. The other channels are closed forming evanescent modes whose role is crucially important for BICs. The evanescent modes of waveguide shift the BIC points and "blow out" the BIC modes from the open resonator. Moreover in 3d resonators the evanescent modes play principal role to give rise to the BICs.

In order to illustrate these statements we start with the planar microwave metallic cavity or resonator with the Dirihclet boundary conditions at the walls. Such a system is convenient by that the solutions with different polarizations, TE and TM, are separated [98]. The total system can be viewed as consisted of three subsystems: two semi infinite planar waveguides and rectangular plane resonator. In each subsystem the solution obeys the Helmgoltz equation [75]

$$-\nabla^2 \psi(x, y) = \frac{\omega^2}{c^2} \psi(x, y). \tag{51}$$

In what follows all quantities are measured in terms of the light velocity c. This equation is completely equivalent to the case of electron transmission in microwave waveguides

$$-\nabla^2 \psi(x, y) = \frac{2m^* E}{\hbar^2} \psi(x, y)$$

where m^* is the effective electron mass with energy E. In the plane waveguides the solutions are given by TE propagating waves [98]

$$\psi_p(x, y) = \sqrt{\frac{1}{2\pi k_p}} \exp(ik_p x)\phi_p(y)$$
 (52)

$$\phi_p(y) = \sqrt{2}\sin(\pi py) \tag{53}$$

with the eigenfrequency spectra

$$\omega^2 = k_p^2 + \pi^2 p^2, p = 1, 2, 3, \dots$$
 (54)

Here $\psi_p(x, y) = E_z(x, y)$ responses for the electric field component of EM field. The integer p numerates channels which are opened for increasing of the frequency as shown in Fig. 7. Other components of EM field can be easily

expressed through $\psi(x, y)$ by use of the Maxwell equations [98]. The solutions inside the closed rectangular resonator are the following

$$\psi_{mn}(x,y) = 2\sqrt{\frac{1}{L_x L_y}} \sin\left(\frac{\pi mx}{L_x}\right) \sin\left(\frac{\pi ny}{L_y}\right)$$
 (55)

with the discrete eigenfrequencies

$$\omega_{m,n}^2 = \frac{\pi^2 m^2}{L_v^2} + \frac{\pi^2 n^2}{L_v^2} \tag{56}$$

where m and n are integers. Here and further all dimensional quantities are measured in the terms of the waveguide's width d, i.e., d = 1. These eigenfrequencies as dependent on the resonator width W are shown in Fig. 8. In respect to

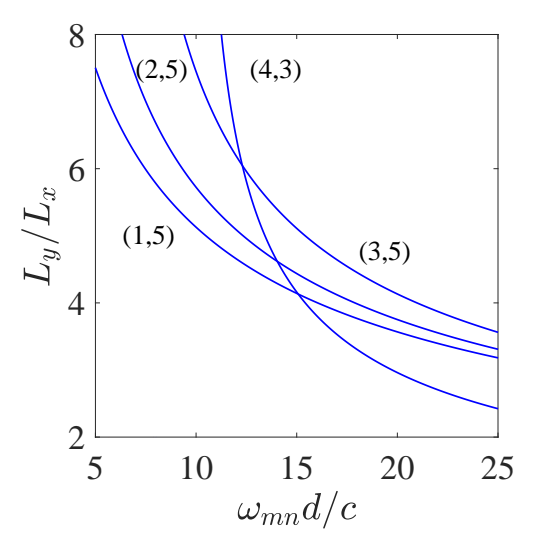


Figure 8: Selected frequencies (56) of the closed rectangular resonator vs width L_{γ} . $E_0 = c^2/d^2$.

the non Hermitian effective Hamiltonian approach it is important to note that the Helmgoltz equation (51) one by one is equivalent to the quantum mechanical description of the electron transmission through quantum dots with attached quantum wires. The squared frequency can be expressed as the quantum energy $E = \omega^2$ and the electric field directed perpendicular to metallic planes is equivalent to the quantum wave function [75] $E_z = \psi(x, y)$. However the effective non Hermitian Hamiltonian (3) is to be modified with account of dispersion properties of microwave waveguides (54) as follows [70, 72]:

$$\widehat{\mathcal{H}}_{eff} = \widehat{\mathcal{H}}_B - i \sum_{C=L,R} \sum_p W_{Cp} W_{Cp}^{\dagger}, \tag{57}$$

where the matrix elements of the coupling matrix elements between the m, n-th eigenmode of the closed resonator and the p-th propagation channel of the C-th waveguide equal

$$W_{mn;pC} = \sqrt{\frac{1}{\pi k_p}} \int_{-1/2}^{1/2} dy \sin\left(\frac{\pi py}{d}\right) \frac{\partial \psi_{mn}(x,y)}{\partial x} \bigg|_{x=x_C},$$
 (58)

 $C = L_x R$ enumerates the interfaces between the left and right waveguides shown in Fig. 1 by dashed lines $x_L = -L_x/2$, $x_R = L_x/2$. We pay attention that the overlapping is given by derivatives of the eigenfunctions of closed resonator over the transmission direction but not the eigenfunctions themselves which equal zero at the boundaries shown in Fig. 1 by dash lines. In the present case of planar resonator this direction is the x-direction as shown in Fig. 1. For the case of TM waves the magnetic field $H_z(x, y)$ serves as the wave function $\psi(x, y)$ with the Neumann boundary conditions at the metallic walls of waveguide that makes the problem fully equivalent to transmittance of

acoustic waves in hard wall resonator. In that case the form of the effective Hamiltonian remains the same but the coupling matrix elements takes the following form [71, 72]

$$W_{mn;pC} = \sqrt{\frac{k_p}{\pi}} \int_{-1/2}^{1/2} dy \sin\left(\frac{\pi py}{d}\right) \psi_{mn}(x,y) \bigg|_{x=x_c}.$$
 (59)

The S-matrix is given [67, 77]

$$S_{CC'} = \delta_{CC'} - 2i\widehat{W}^C \frac{1}{E - \widehat{H}_{eff}} \widehat{W}^{C'}.$$

$$(60)$$

In Fig. 9 we show the transmittance in the first open channel vs incident frequency $E = \omega^2$ and the width of resonator W.

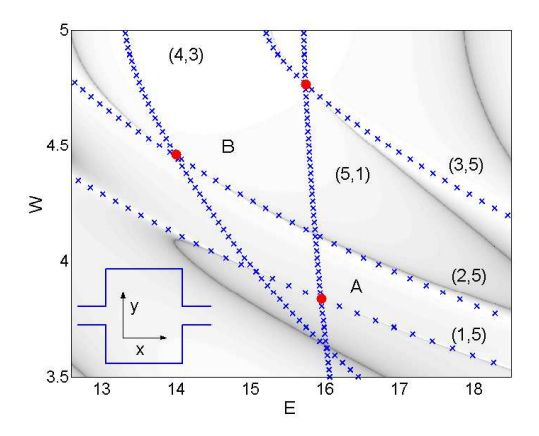


Figure 9: The transmittance in Log scale through the rectangular resonator shown in the inset versus energy $E = \omega^2$ and width W of the resonator (in terms of the width of the lead). The dark areas correspond to low transmittance. The length of the resonator along the transport axis equals 4. The eigenfrequencies of the closed billiard are marked by crosses. The positions of the BICs are shown by closed red circles. The patterns of the two BICs A and B are shown in Fig. 11.

In the framework of this formalism, the positions and decay widths of the resonance states follow from the complex eigenvalues of the non-Hermitian effective Hamiltonian

$$\hat{H}_{eff}|\lambda\rangle = z_{\lambda}|\lambda\rangle \tag{61}$$

where $z_{\lambda} = E_{\lambda} - i\gamma_{\lambda}/2$. The biorthogonal eigenstates are normalized as $(\lambda | \lambda') = \delta_{\lambda,\lambda'}$, where $(\lambda |$ is given by transpose of $|\lambda|$. Similar to the two-level approach for description of BICs in Section 3 the BIC of the present formalism is given by those eigenstate of the effective Hamiltonian, whose eigenvalue is real. However as distinct of phenomenological case by Friedric and Wintgen [7] (see also Ref. [12]) the coupling matrix elements (59) are frequency dependent through Eq. (54). Then the resonant positions and widths are obtained by solving the corresponding fixed-point equations [68]

$$E_{\lambda} = Re(z_{\lambda}(E_{\lambda})), \quad 2\gamma_{\lambda} = -Im(z_{\lambda}(\gamma, E_{\lambda})). \tag{62}$$

Moreover the rank of matrix of the effective Hamiltonian is defined by number of the eigenmodes of closed resonator whose number rigorously speaking is infinite. In order to solve the eigenvalue problem one has to decimate the matrix however a convergence of the matrix of the effective Hamiltonian is controversial for the Dirichlet BC [71]. In practice we explore the tight-binding approach for the effective Hamiltonian [70] which is equivalent to finite difference method of solution of the Helmholtz equation (51). The one half of eigenvalues of the effective non Hermitian Hamiltonian (57) are real and correspond to the symmetry protected BICs because they are antisymmetric relative to $y \rightarrow -y$ and therefore have zero couplings (58) with the first channel continuum p = 1 provided that $\omega^2 < 4\pi^2$. The second half of the eigenvalues is complex and correspond to resonances for wave transmission through the rectangular resonator. However a very few of these complex eigenvalues have a tendency to acquire zero imaginary parts for variation of the

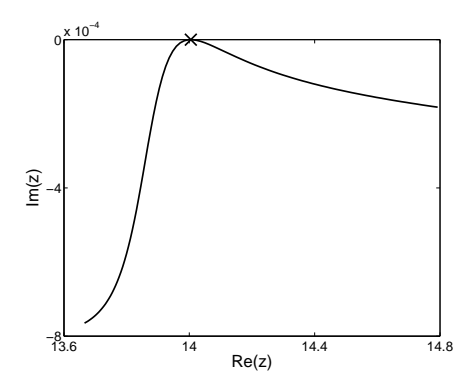


Figure 10: The evolution of resonance width Im(z) and position Re(z) of one of the two resonance states in the vicinity of the BIC B in Fig. 9. Im(z) vanishes at $L_y = 4.45$ (marked by a cross). The widths of the other resonance states are much larger and are not shown here.

width of the resonator at the vicinity of those points where a degeneracy of the eigenfrequencies (56). One of such events is shown in Fig. 10 where other eigenfrequencies are excluded in order to avoid obscure picture.

One can see from Fig. 9 that these BICs are located in the very close vicinity to the points of degeneracy of the eigenmodes of the close resonator. Indeed when the eigenmodes, say ψ_1 become degenerate one can superpose the eigenmodes as $\psi = a_1\psi_1 + a_2\psi_2$. Although each eigenmode is coupled with the continuum $|C\rangle$ via the coupling constants $W_1 = \langle C|\psi_1\rangle \neq 0$ and $W_2 = \langle C|\psi_2\rangle \neq 0$ the coupling of the superposed state $W = \langle C|\psi\rangle = a_1W_1 + a_2W_2$ can be cancelled by a proper choice of the superposition coefficients a_1 and a_2 [17]. Then this state ψ becomes the BIC which is decoupled from the waveguides for the case $E < 4\pi^2$.

The BIC function. In general case the scattering wave function obeys the following equation [70, 71]

$$\psi_{L}(x,y) = \frac{1}{\sqrt{4\pi k_{1}}} \left[e^{ik_{1}x} \phi_{1}(y) + \sum_{p} S_{1L;pL} e^{-ik_{p}x} \phi_{p}(y) \right], \quad x < -L_{x}/2,$$

$$\psi_{B}(x,y) = -i \sum_{m'n'} G_{mn;m'n'} \sqrt{\frac{k_{p=1}}{\pi}} W_{m'n';1L} \psi_{m'n'}(x,y), \quad -L_{x}/2 < x < L_{x}/2,$$

$$\psi_{R}(x,y) = \sum_{p} \frac{1}{\sqrt{4\pi k_{p}}} S_{1L;pR} e^{ik_{p}x} \phi_{p}(y), \quad x > L_{x}/2,$$
(63)

where $S_{pC,p'C'}$ are components of the S-matrix (60) and the Green function \widehat{G} is the inverse of the matrix $\omega^2 - \widehat{H}_{eff}$. So, inside the resonator the wave function is given by the Lippmann-Schwinger equation [70, 71]

$$(\omega^2 - \widehat{H}_{eff})|\psi_B\rangle = \widehat{W}_{Lp=1}a_{L,p=1}^*|L, p = 1\rangle$$

where the waveguide states are given by incoming wave amplitude $a_{L,p=1}^+$ for the present case of 2d wave transmission shown in inset of Fig. 9. We imply that the wave incomes through the left waveguide. Eq. (64) has unambiguous solution until the operator at the left can be inverted. However, if

$$\|\omega^2 - \hat{H}_{eff}\| = 0, (64)$$

the inverse operator does not exist, and the solution becomes ambiguous.

Such a precedent was revealed in a periodical structure (grating slab) [99] and is a consequence of bound states in the diffraction continuum [31, 32]. If Eq. (64) is fulfilled, then the solution of Eq. (64) can be presented as superposition [94]

$$|\psi_B\rangle = \alpha |BIC\rangle + |\psi_p\rangle,\tag{65}$$

where the first part is the solution of the homogeneous equation

$$(\omega^2 - \hat{H}_{eff})|BIC\rangle = 0 \tag{66}$$

while the second contribution is the particular solution of Eq. (64). In the presentation of eigenstates (61) Eq. (64) takes the following form

$$\prod_{\lambda} (\omega^2 - z_{\lambda}) = 0. \tag{67}$$

Obviously, Eq. (64) is fulfilled if some of complex eigenvalues becomes real, i.e. at the BIC point. Then the necessary and sufficient condition for existence of solution of the equation (64) is that the vector [94]

$$\langle BIC|\psi_p\rangle = 0. \tag{68}$$

This equation has clear physical meaning of that the BIC solution is orthogonal to the solution which propagates in waveguide, therefore can not leakage from the cavity.

It might be seemed that the BIC solution (43) can be presented by only those eigenfunctions (55) which undergo degeneracy, events of which are shown in Fig. 8. In particular, let us consider the eigenmodes $\psi_{4,3}$ and $\psi_{2,5}$ with corresponding eigenfrequencies

$$\omega_{4,3}^2 = \omega_a^2 = \frac{4^2}{L_x^2} + \frac{3^2}{L_y^2},$$

$$\omega_{2,5}^2 = \omega_b^2 = \frac{2^2}{L_y^2} + \frac{5^2}{L_y^2}.$$
(69)

All dimensional units are measured in term of the waveguide width d and frequency is measured in term of $\sqrt{E_0} = \frac{c}{d}$. The degeneracy point is given by relation $\frac{L_y}{L_x} = \frac{2}{\sqrt{3}}$ and respectively the BIC frequency equals $\omega_c = \frac{4\pi}{L_x} \sqrt{1 + \frac{27}{64}}$. In numerics we have chosen $L_x = 4$ that gives $\omega_c = 3.746$. Then the coupling matrix elements (58) equal

$$W_{4,3;1L} = W_{4,3;1R} = W_a = \sqrt{\frac{2}{k_1}} \frac{8\pi}{L_x^{3/2} L_y^{1/2}} \int_{-1/2}^{1/2} dy \cos(\pi y) \cos(3\pi y/L_y) \approx 0.618,$$

$$W_{2,5,1L} = W_{2,5;1R} = W_b = \sqrt{\frac{2}{k_1}} \frac{4\pi}{L_y^{3/2} L_y^{1/2}} \int_{-1/2}^{1/2} dy \cos(\pi y) \cos(5\pi y/L_y) \approx 0.4.$$

Thus, the BIC solution in two-level approximation can be written as the linear superposition, at least, at the point of degeneracy $\omega = \omega_c$

$$\psi_{BIC}(x, y) = \psi_0(W_b \psi_a(x, y) - W_a \psi_b(x, y)) \tag{70}$$

where indices 4, 3 and 2, 5 are absorbed by the indices a and b respectively. One can easily verify this function is orthogonal to the first continuum of both waveguides given by p = 1 and turns to zero at the boundaries $x = \pm L_x/2$ and therefore is localized inside the resonator. The matrix of the effective Hamiltonian (57) takes the following form

$$\begin{pmatrix} \omega_{1}^{2} - 2iW_{1}^{2} & -2iW_{1}W_{2} & \dots & -2iW_{1}W_{a} & -2iW_{1}W_{b} \\ -2iW_{1}W_{2} & \omega_{2}^{2} - 2iW_{2}^{2} & \dots & -2iW_{2}W_{a} & -2iW_{2}W_{b} \\ \vdots & \vdots & \ddots & \vdots & \vdots \\ -2iW_{1}W_{a} & -2iW_{2}W_{a} & \dots & \omega_{a}^{2} - 2iW_{a}^{2} & -2iW_{a}W_{b} \\ -2iW_{1}W_{b} & -2iW_{2}W_{b} & \dots & -2iW_{b}^{2} & \omega_{b}^{2} - 2iW_{a}W_{b} \end{pmatrix} = 0.$$
 (71)

Equation for the BIC takes the following form

$$\begin{bmatrix} \frac{\omega_1^2 - \omega^2}{2iW_1^2} + 1 & 1 & \dots & 1 & 1\\ 1 & \frac{\omega_2^2 - \omega^2}{2iW_2^2} & \dots & 1 & 1\\ \vdots & \vdots & \ddots & \vdots & \vdots\\ 1 & 1 & \dots & \frac{\omega_a^2 - \omega^2}{2iW_a^2} & 1\\ 1 & 1 & \dots & 1 & \frac{\omega_b^2 - \omega^2}{2iW_s^2} \end{bmatrix}$$
 (72)

One can see that at the point of degeneracy $\omega_a = \omega_b$ and $\omega = \omega_a$ the determinant (72) turns to zero to realize the BIC as the linear superposition of degenerate states (70).

Which is role of evanescent modes? First, we show that the evanescent modes shift the BIC point. The effective Hamiltonian (57) can be rewritten as follows for $\omega^2 < 4\pi^2$

$$\widehat{H}_{eff} = \widehat{\widetilde{H}}_B - 2i\widehat{W}_1\widehat{W}_1^{\dagger},\tag{73}$$

where

$$\widehat{\widetilde{H}}_B = \widehat{H}_B - 2 \sum_{p>1} \widehat{\widetilde{W}}_p \widehat{\widetilde{W}}_p^{\dagger}, \tag{74}$$

where the coupling matrix $\widehat{W}_{p=1}$ is defined by Eq. (58) or Eq. (59) while the coupling matrix $\widehat{W}_{p>1}$ originated from the evanescent modes and equal

$$\widetilde{W}_{mn;p>1} = \sqrt{\frac{1}{\pi |k_p|}} \int_{-1/2}^{1/2} dy \sin\left(\frac{\pi py}{d}\right) \frac{\partial \psi_{mn}(x,y)}{\partial x} \bigg|_{x=\pm L_y/2}.$$
 (75)

The factor 2 in Eqs. (73) and (74) is the result of equal contribution of both left and right waveguides. The matrix $\widehat{\widetilde{H}}_B$ is Hermitian and can be interpreted as the effective Hamiltonian of the cavity modified by evanescent modes. Substituting modified eigenvalues into (72) we obtain that points of degeneracy of them define the exact BIC points.

Second, the approximate BIC solution (70) turns to zero at boundaries between the resonator and waveguides $x = \pm L_x/2$. The exact BIC solution defined by Eq. (66) which can be expressed in series of the eigenfunctions of the closed resonator

$$\psi_{BIC}(x,y) = \sum_{mn} a_{mn} \psi_{mn}(x,y) \tag{76}$$

where the expansion coefficients are given by eigenvector of Eq. (66). Although each eigenfunction $\psi_{mn}(x = \pm L_x/2, |y| < 1/2) = 0$ the BIC solution (76) is to be sewed with the evanescent modes in the waveguides which exponentially decay when we move away from the boundary of the closed resonator

$$\sum_{mn} a_{mn} \psi_{mn}(x = \pm L/2, |y| < 1/2) = \sum_{p>1} \frac{a_p}{\sqrt{4\pi k_p}} \phi_p(y) \approx \frac{a_2}{\sqrt{4\pi k_2}} \phi_2(y).$$
 (77)

We pay attention that if we restricted by only two eigenfunctions which undergo degeneracy in the vicinity of the BIC point the left hand expression in Eq. (77) would turn to zero. Only due to infinite series over the eigenfunctions the left hand expression (77) differs from zero. Thus, the second role of the evanescent modes is in exponential weak blowing of the BIC solution into waveguides that provides smooth behavior of the BIC solution as seen from Fig. 11. These BIC solutions

56) with sufficiently large rank of the effective Hamiltonian. Thus, there are two ii

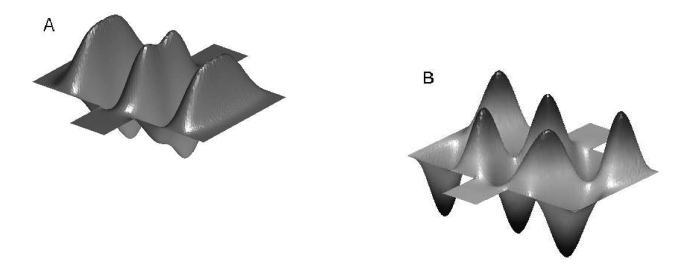


Figure 11: The patterns of the two BICs A and B marked in Fig. 9 by bold circles.

from the resonator due to coupling to the evanescent modes as seen from Fig. 11. A degree of the overflowing is given by the exponential contribution of the first evanescent mode $\exp(-\sqrt{(2\pi)^2 - \omega^2}(x - L_x/2))$ in the right waveguide. The same holds in the left waveguide however for x < -L/2. Second, the BIC point is shifted relative to points of degeneracy of eigenmodes of the closed resonator because of contribution in the effective Hamiltonian (74). Details of these effect will be given below for the 3d resonators where the contribution of evanescent modes has principal importance for existence of BICs.

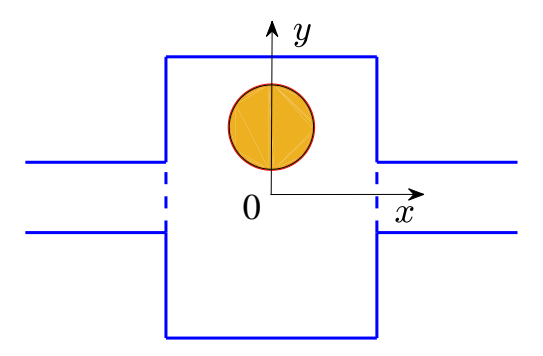


Figure 12: (Color online) Dielectric or metallic disk inside the rectangular open resonator.

6. Accidental BICs in the Sinai shaped open cavity

The rectangular cavity is an example of integrable system when the variables x and y are separated that reduces the eigenvalue problem to the one-dimensional one with multiplicative eigenfunctions (55). Because of that for variation of one of the scales of the resonator, say width W, we have multiple events of degeneracy each of which gives rise to BICs in the Friedrich-Wintgen scenario as it was described in previous section. In fact there are only a few integrable resonators, elliptic and equilateral triangle which are specified by Poisson distribution of the nearest distances between eigenlevels. All the rest falls into non integrable whose eigenlevels undergo avoided crossings for variation of some parameter with the Wigner distribution and form so called chaotic billiards [75]. The Bunimovich and Sinai billiards are the well known examples of chaotic billiards. Experimentally it is easy to transform the integrable billiard into the chaotic one by embedding of dielectric or metallic disk inside the plane rectangular cavity as sketched in Fig. 12. Then the FW mechanism of the BIC due to degeneracy of eigenstates of closed billiard is not applicable. However there is another way to realize the BIC by decoupling of an individual eigenmode of the Sinai billiard from the the first continuum of waveguides [50, 55]. For that we smoothly deform the eigenmodes by, for example, variation of radius or position of disk inserted inside the rectangular cavity. The effect of disk can be described by a circular potential perturbation

$$V(x,y) = V_g \exp\left[-\frac{(x-x_0)^2 + (y-y_0)^2}{R^2}\right]$$
 (78)

added into the effective Hamiltonian (57). To be specific we consider the Neumann boundary conditions because of good convergence of the results with growth of rank of the matrix \widehat{H}_{eff} for low lying eigenfrequencies [71].

In what follows we fix the radius R = 1.5 and position of circular potential at $x_0 = 0$, $y_0 = 1$ in terms of the waveguides width d and vary the height V_g of the potential (78) that effectively varies the radius of the circular potential. Because of symmetry of full system relative to $x \to -x$ the continua of both waveguides are identical. Respectively we have identical coupling matrix elements of the Sinai resonator with waveguide continua

$$W_{b,pC} = \sqrt{\frac{1}{k_p}} \int_0^d dy \phi_p(y) \frac{\partial \psi_b(x,y)}{\partial x} \bigg|_{y=\pm L/2}, \tag{79}$$

where C = L, R enumerates the interfaces between the left and right waveguides shown in Fig. 12 by dashed lines, ψ_b are the eigenfunctions of the closed Sinai billiard.

The eigenfunctions are classified as even and odd $\psi(x,y) = \pm \psi(-x,y)$. Respectively, the eigenvalues in each irreducible representation undergo avoided crossings with variation of V_g as illustrated in Fig. 13. For clarity we show some patterns of the eigenfunctions at $V_g = 50$ in Fig. 13. One can see that the eigenfunctions are depleted inside by the potential (78) at $V_g = 50$. A variation of another parameter of the potential (78), for example, the radius or position shows a similar result. Thus, we have no degeneracy of the eigenfunctions of the same irreducible representation in the chaotic Sinai resonator.

Fig. 14 shows the transmittance calculated via Eq. (60). In order the reader can observe that peaks of the transmittance follow the eigenvalues of the closed Sinai resonator we reduce the coupling between the waveguides

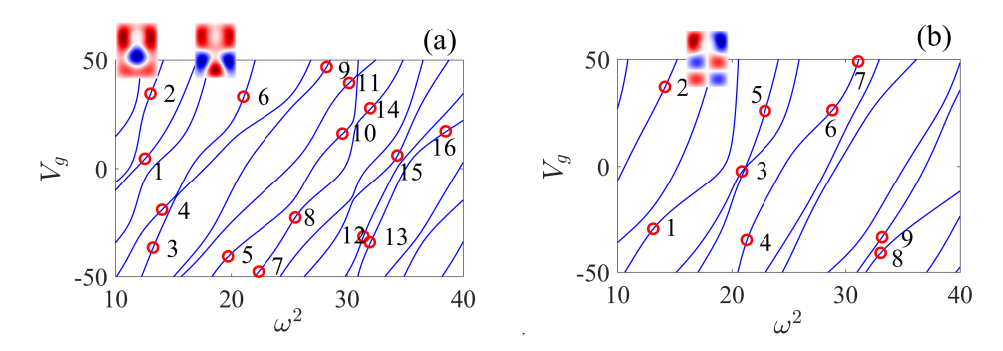


Figure 13: (Color online) Eigenvalues and eigenfunctions of the soft Sinai resonator vs height of the potential (78). Insets show a few patterns of corresponding eigenfunctions are even (a) and odd (b) relative to $x \to -x$. Open circles mark the BIC points.

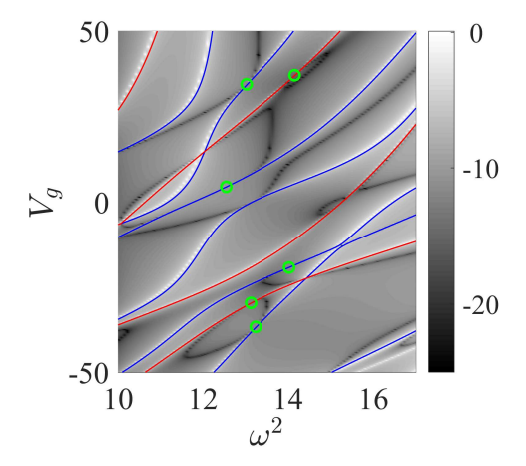


Figure 14: Transmittance of the Sinai resonator in Log scale vs V_g (effective radius of the circular hole shown in Fig. 12) and incident frequency. The BICs are shown by open circles.

and the resonator by implementation of diaphragms between the waveguides and the billiard [100] that narrows transmission peaks. The BIC occurs if the resonance width turns to zero which are given by the imaginary part of the complex eigenvalues of the effective non-Hermitian Hamiltonian

$$\widehat{H}_{eff} = \widehat{H}_B + V_g - i \sum_{C=L,R} \sum_p \widehat{W}_{C,p} \widehat{W}_{C,p}^{\dagger}, \tag{80}$$

where $\widehat{\mathcal{H}}_B$ is the Hamiltonian of closed rectangular resonator, and $\widehat{W}_{C,p}$ are columns of matrix elements (79) labelled by the eigenstate indices b. Numerically computed evolution of the resonant widths is presented in Fig. 15 which shows multiple events of the resonant widths turning to zero, i.e., BICs in the Sinai resonator. The even BICs sorted by their energies are shown in Fig. 13 (a) by open circles. Respectively the odd BICs are shown in Fig. 13 (b). Besides these BICs one can see in Fig. 15 numerous symmetry protected BICs at the point $V_g = 0$ which are the eigenfunctions of the rectangular resonator antisymmetric relative to $y \to -y$ for $\omega < 2\pi$. And therefore they are incompatible with the symmetric propagating mode in the first channel p = 1 (53).

Fig. 14 clearly demonstrates that the BIC points are positioned at those points in the parametric space of E and V_g where the transmission zero coalesces with the transmission unit similar to the FW BICs [17] illustrating the collapse of Fano resonance [34]. However in the Sinai billiard the BICs occur accidentally under variation of the circular potential (78) that changes the eigenfunctions of the closed Sinai resonator as shown in insets in Fig. 13. That in turn changes the coupling matrix elements (79) so that some of them can turn to zero as illustrated in Fig. 16. That is a mechanism of the accidental BICs patterns shown in Figs. 17 and 18. These Figures also depict the modal expansion

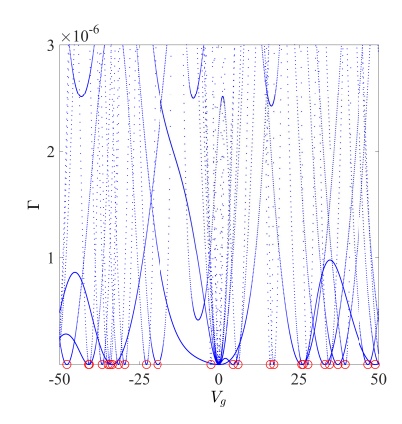


Figure 15: Evolution of the resonant widths for variation of the potential. Red open circles mark BICs.

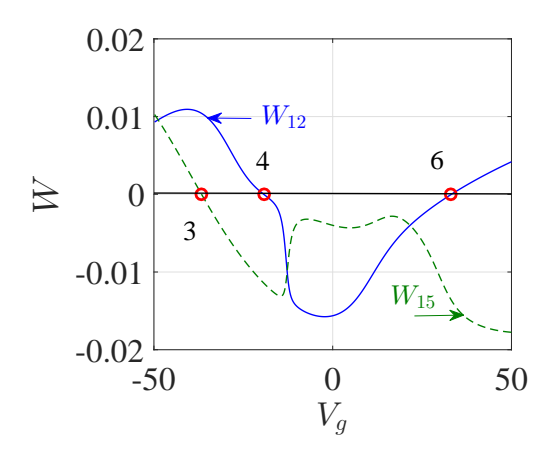


Figure 16: Evolution of the coupling matrix element (79) with V_g .

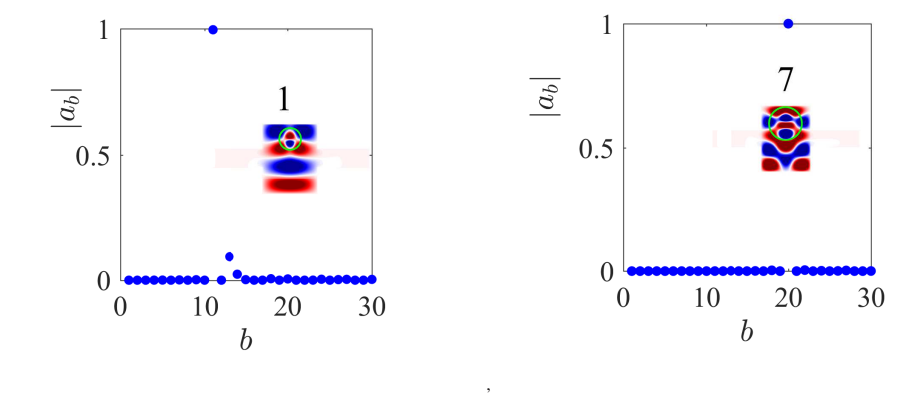
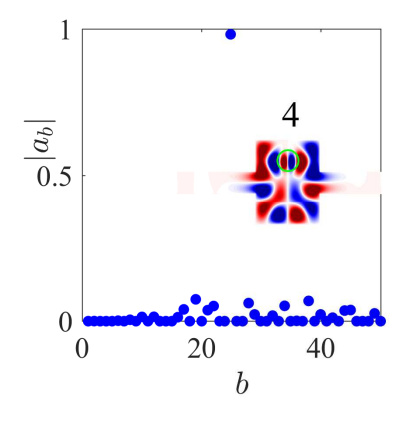


Figure 17: (Color online) Patterns of even BICs enumerated according to Table 2 with coefficients of the modal expansions. Position of potential (78) is shown by green circle.



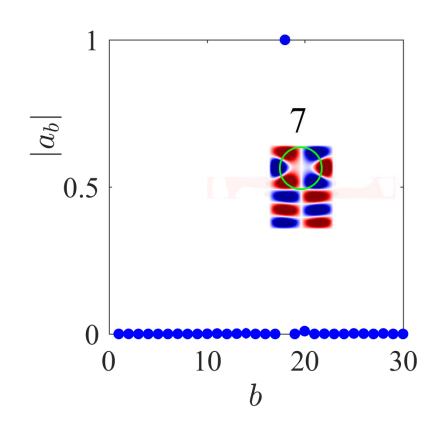


Figure 18: (Color online) Patterns of odd BICs enumerated according to Table 3 with coefficients of the modal expansions.

coefficients $|a_b|$ of BICs over the eigenmodes of the closed Sinai resonator

$$\psi_{BIC}(x,y) = \sum_{b} a_b \psi_b(x,y). \tag{81}$$

One can see that indeed basically one eigenfunction contributes into the BIC mode. There is also background of other eigenfunctions which is a result of contribution of evanescent modes into the effective Hamiltonian (see discussion in previous section).

In what follows we will prove that if one of coupling matrix elements $W_{b,p=1}$ vanishes then the accidental BIC occurs embedded into the continuum of the first propagating channel p=1 of both waveguides C=L,R. Let us choose, for example, the eigenfunction of the closed billiard, say b=3, whose coupling with the first channel p=1 turns to zero. Then we can write the coupling matrix (79) as follows

$$W_{b,1} = (W_1 \ W_2 \ 0 \ W_4 \ \dots). (82)$$

Because of symmetry relative $x \to -x$ the coupling matrix (82) is invariant relative to choice of waveguides C = L, R. Then there is a vector

$$\psi_3^+ = (0 \ 0 \ 1 \ 0 \ \dots) \tag{83}$$

which is the eigen null vector of the matrix $WW^+\psi_3 = 0$. On the other hand, the vector (83) is the eigenvector of the closed billiard with the Hamiltonian

$$\widehat{H}_{B} = \begin{pmatrix} \omega_{1}^{2} & 0 & 0 & 0 & \cdots \\ 0 & \omega_{2}^{2} & 0 & 0 & \cdots \\ 0 & 0 & \omega_{3}^{2} & 0 & \cdots \\ 0 & 0 & 0 & \omega_{4}^{4} & \cdots \\ \vdots & \vdots & \vdots & \ddots \end{pmatrix}.$$

$$(84)$$

with the eigenfrequency ω_3 . Thus the null eigenvector (83) is the eigenstate of the effective non-Hermitian Hamiltonian (80) with real eigenfrequency ω_3 , and therefore is the BIC with this frequency. That result does not depend on the other coupling matrix elements in (82). Following Refs. [31, 32] we define such BICs as accidental. Note that conclusion is correct in neglecting of the evanescent modes of waveguides. The contribution of evanescent modes can be performed as it was done in Section 5. However in this case the eigenstate (83) ceases to be the eigenstate of the effective Hamiltonian. As a result as Fig. 18 (a) shows the accidental BIC is blowing off the Sinai billiard and modal expansion shows noticeable background of all other eigenmodes of the billiard.

Table 2: BICs even relative to $x \to -x$ marked by open circles in Fig. 13 (a).

Number of the even BIC	E	V_g
1	12.550	4.5
2	13.029	34.45
3	13.244	-36.65
4	14.026	-19.2
5	19.709	-40.7
6	21.025	33.05
7	22.355	-47.7
8	25.541	-22.8
9	28.236	46.7
10	29.608	16.05
11	30.181	39.35
12	31.418	-31.55
13	31.960	-34.2
14	32.002	27.75
15	34.333	6.00
16	38.495	17.15

Table 3: BICs odd relative to $x \to -x$ marked by open circles in Fig. 13 (b).

Number of the odd BIC	E	V_g
1	13.133	-29.6
2	14.155	37.1
3	20.882	-2.4
4	21.307	-34.8
5	22.927	25.85
6	28.844	26.25
7	31.099	48.95
8	33.063	-40.9
9	33.189	-33.5

7. The cylindrical resonator with non-axisymmetric waveguides. The twisted BICs.

The aim of this and next sections is to demonstrate nontrivial role of the waveguides whose attachment breaks the symmetry of the closed resonators with nontrivial BICs embedded into continua of these waveguides. For example, the closed cylindrical resonator with the radius R and length L is the typical the textbook case [98] which allows separation of variables in the cylindrical system of coordinates. If to attach cylindrical waveguides coaxially as shown in Fig. 19 (a) the axial symmetry of the total open system is preserved. We skip this case of coaxial connected waveguides where the FW BICs are accessed via variation of the length of the resonator L [101] similar to the section 5 (planar rectangular resonators). However if one of waveguides is shifted off the symmetry axis of the resonator as shown in Fig. 19 (b) the axial symmetry of the total system breaks. We consider the case of non-axisymmetric waveguides which are identical but are attached to the resonator by different angles so that the waveguides are unwrapped by angular difference $\Delta \phi$ as shown in Fig. 19. That does not change strength of coupling matrix elements with continua but differ the continua by phase. We show that nevertheless the BICs exist but have to be twisted by the angle $\Delta \phi$.



Figure 19: Cylindrical resonator with two (a) coaxially and (b) non coaxially attached non-axisymmetric cylindrical waveguide. The input waveguide can freely move along the resonator axis and rotate about the symmetry axis of resonator.

The Helmholz equation (51) can be applied for acoustic transmission through duct-cavity structures in hard wall approximation. The equation takes the following form in the cylindrical system of coordinates

$$\left[\frac{\partial^2}{\partial r^2} + \frac{1}{r}\frac{\partial}{\partial r} - \frac{m^2}{r^2} + \frac{\partial^2}{\partial z^2} + \omega^2\right]\psi = 0,$$
(85)

for the non-dimensional velocity potential ψ where the non-dimensional coordinates r and z are normalized by the waveguide radius r_w . The dimensionless frequency ω is defined through the dimensional frequency $\widetilde{\omega}$ as follows $\omega = \widetilde{\omega} r_w/c_0$ and c_0 is the sound speed.

The propagating modes in the sound hard cylindrical waveguides with Neumann boundary conditions are described by

$$\psi_{pq}(\rho, \alpha, z) = \psi_{pq}(\rho) \frac{1}{\sqrt{2\pi k_{pq}}} \exp(ip\alpha + ik_{pq}z),$$

$$\psi_{pq}(\rho) = \begin{cases} \frac{\sqrt{2}}{J_0(\mu_{0q})} J_0(\mu_{0q}\rho), p = 0, \\ \sqrt{\frac{2}{\mu_{pq}^2 - p^2}} \frac{\mu_{pq}}{J_p(\mu_{pq})} J_p(\mu_{pq}\rho), p = 1, 2, 3, \dots, \end{cases}$$
(86)

where ρ , α are the polar coordinates shown in Fig. 20, μ_{pq} is the q-th root of equation

$$\left. \frac{dJ_p(\mu_{pq}\rho)}{d\rho} \right|_{\rho=1} = 0$$

imposed by the Neumann boundary condition on the walls of sound hard cylindrical waveguide.

$$k_{pq}^2 = \omega^2 - \mu_{pq}^2 \tag{87}$$

11	it-on frequencies and corresponding snapes of propagating modes in the circula						
	channel cut-off frequency		indices	mode shape			
	1	0	p = 0, q = 1				
	2	1.84118	$p = \pm 1, q = 1$				
	3 3.0542		$p = \pm 2, q = 1$				
	4	3.831706	p = 0, q = 2				

Table 4: Cut-off frequencies and corresponding shapes of propagating modes in the circular waveguide.

The dimensional quantities ρ , z, k_{pq} are measured in terms of the radius of the waveguide ρ and frequency is measured in the terms of the ratio s/ρ where s is the sound velocity. The propagating bands degenerate with the respect to the sign of azimuthal index and are classified by two indices, the azimuthal index $p=0,\pm 1,\pm 2,\ldots$ and radial index $q=1,2,3,\ldots$ Profiles of propagating functions $\psi_{pq}(\rho)\cos p\alpha$ are depicted in Table 4.

The Hilbert space of the closed cylindrical resonator is given by the following eigenmodes

$$\Psi_{mnl}(r,\phi,z) = \psi_{mn}(r)\sqrt{\frac{1}{2\pi}}\exp(\mathrm{i}m\phi)\psi_l(z),\tag{88}$$

where

$$\psi_{mn}(r) = \begin{cases} \frac{\sqrt{2}}{RJ_0(\mu_{0n}R)} J_0(\frac{\mu_{0n}r}{R}), m = 0\\ \sqrt{\frac{2}{\mu_{mn}^2 - m^2}} \frac{\mu_{mn}}{RJ_m(\mu_{mn}R)} J_m(\frac{\mu_{mn}r}{R}), m = 1, 2, 3, \dots, \end{cases}$$

$$\psi_l(z) = \sqrt{\frac{2-\delta_{l,1}}{L}} \cos[\pi(l-1)z/L],$$
(89)

 $l = 1, 2, 3, \dots$ and z is measured in terms of the waveguide radius. The corresponding eigenfrequencies are

$$\omega_{mnl}^2 = \left[\frac{\mu_{mn}^2}{R^2} + \frac{\pi^2 (l-1)^2}{L^2} \right] \tag{90}$$

where μ_{nm} is the n-th root of the equation $\frac{dJ_m(\mu_{mn}r)}{dr}\Big|_{r=R} = 0$ which follows from the Neumann BC on the walls of hard cylindrical resonator.

The matrix elements of \hat{W} are given by overlapping integrals [71, 102]

$$W_{mnl;pq}^{C} = \int_{\Omega_{C}} \rho d\rho d\alpha \psi_{pq}(\rho, \alpha) \Psi_{mnl}^{*}(r, \phi, z = z_{C})$$

$$= \int_{0}^{2\pi} d\alpha \int_{0}^{1} \rho d\rho \psi_{pq}(\rho, \alpha) \Psi_{mnl}^{*}(r(\rho, \alpha), \phi(\rho, \alpha), z_{C})$$

$$= \psi_{l}(z_{C}) \int_{0}^{2\pi} d\alpha \int_{0}^{1} \rho d\rho \psi_{pq}(\rho, \alpha) \psi_{mn}^{*}(r(\rho, \alpha), \phi(\rho, \alpha)), \tag{91}$$

where $\Omega_{C,C=L,R}$ are interfaces positioned at $z_C = 0, L$. Integration is performed over circular cross section of the attached waveguides as shown in Fig. 20. One can link the polar coordinates of the resonator with that of the immovable waveguide

$$r\sin\phi = \rho\sin\alpha, r\cos\phi = r_0 + \rho\cos\alpha$$

where r_0 is the distance between the axes of the waveguide and resonator.

According to Eq. (88) we have

$$\psi_l(z=0) = \sqrt{\frac{2 - \delta_{l,1}}{L}}, \psi_l(z=L) = \psi_l(0)(-1)^{l-1}.$$
 (92)

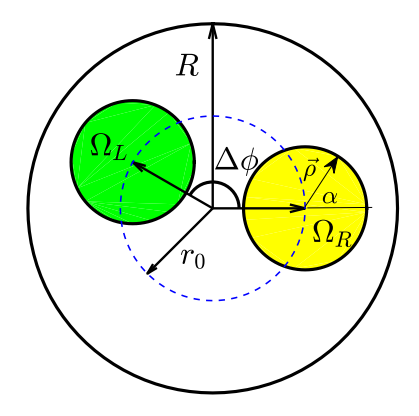


Figure 20: Filled areas show overlapping integration area in the coupling matrix (91).

Substituting (92) into (91) we obtain the following relation between the left and right coupling matrix elements

$$W_{mnl;pq}^{L} = (-1)^{l-1} e^{i(p-m)\Delta\phi} W_{mnl;pq}^{R}.$$
(93)

Therefore the matrix of the effective Hamiltonian takes the following form

$$\langle mnl|\widehat{H}_{\text{eff}}|m'n'l'\rangle = \omega_{mnl}^2 \delta_{mm'} \delta_{nn'} \delta_{ll'}$$

$$-i \sum_{pq} k_{pq} [1 + (-1)^{l+l'} e^{i(m'-m)\Delta\phi}] W_{mnl;pq} W_{m'n'l';pq}^*. \tag{94}$$

The transmittance of sound waves in the p, q propagating channel through the resonator is given by equation [71]

$$T_{pq;pq} = 2ik_{pq} \sum_{mnl} \sum_{m'n'l'} W_{mnl;pq} e^{-im'\Delta\phi} G_{mnl;m'n'l'} W_{m'n'l';p'q'}^*$$
(95)

where

$$\widehat{G} = \frac{1}{\omega^2 - \widehat{H}_{\text{eff}}},\tag{96}$$

that is propagation of waves through the resonator is described by the Green function which is inverse of the matrix $\omega^2 - \hat{H}_{\text{eff}}$ and coupling matrices of the resonator with the input (left) waveguide and the output (right) waveguide. However the most remarkable feature in Eq. (95) is complex phases of the coupling matrix elements between states with different azimuthal indices m and p. As we show below that drastically changes the transmittance.

7.1. Variation over the length of resonator at $\Delta \phi = \pi/4$.

The case of $\Delta \phi \neq 0$ is interesting by that we face with problem of embedding of the BIC into two continua which differ by phase. First, the problem of the BIC residing in a finite number of continua was considered by Pavlov-Verevkin and coauthors [103]. Rigorous statement about the BICs was formulated as follows. The interference among N degenerate states which decay into K non-interacting continua generally leads to the formation of N - K BICs. The equivalent point of view [17] is that the linear superposition of the N degenerate eigenstates $\sum_{n=1}^{N} a_n \psi_n$ can be adjusted to have zero coupling with K different continua in N - K ways by variation of the N superposition coefficients a_n . Respectively, that involve K-parametric avoided crossing. The number of continua can grow due to a number of reasons, for example, non-symmetrically attached waveguides, multiple propagation subbands in the waveguides, or two polarizations of the radiation continuum in case of electromagnetic BICs. Each case puts the problem of searching BICs embedding into many continua on the line of art [31, 55, 59, 104–106].

In what follows we take both waveguides with unit radius shifted relative to the central axis of the resonator with radius R=3 by a distance $r_0=1.5$. We consider transmission in the first channel p=0, q=1 in the frequency domain $0 < \omega < \mu_{11} = 1.8412$ (see Table 2). Although rotation of the waveguide does not alter its propagating modes (continua) it provides the complex phases in the coupling matrix elements of the resonator eigenmodes with the continua as given by Eq. (93). That effects the transmittance as shown in Fig. 21.

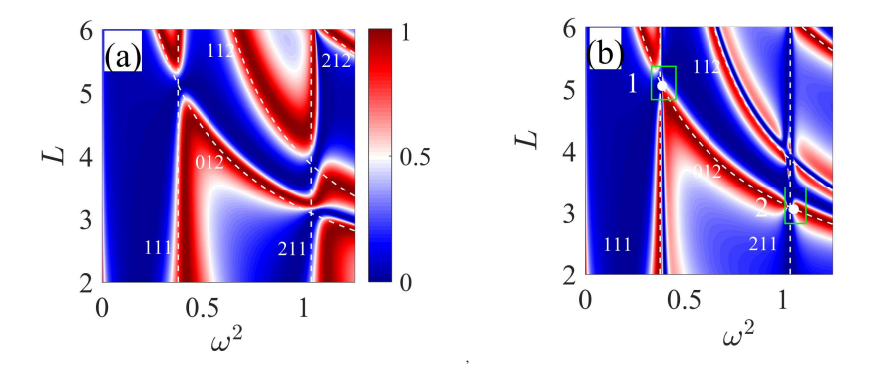


Figure 21: Transmittance of a cylindrical resonator vs frequency and length of the resonator L at (a) $\Delta \phi = 0$ and (b) $\Delta \phi = \pi/4$. Dash lines show eigenlevels of closed resonator with corresponding indices mnl. The positions of the BICs are shown by closed circles.

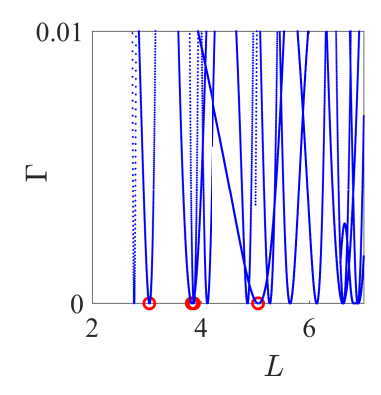


Figure 22: Evolution of resonant widths under variation of the resonator length at $\Delta \phi = \pi/4$. Circles mark BICs listed in Table 3.

As before the BIC points are detected by finding zero resonant width for variation of the resonator's length L at fixed $\Delta \phi = \pi/4$ as shown in Fig. 22. We marked by circles only those BICs which are listed in Table 5 and will be analyzed below. The positions of the BICs and expansions coefficients over the eigen modes of closed resonator (88)

$$\psi_{\rm BIC}(r,\phi,z) = \sum_{mnl} a_{mnl} \Psi_{mnl}(r,\phi,z). \tag{97}$$

are collected in Table 5. Fig. 23 show the 3-th and 4-th BICs marked in Figs. 21 (b) which are the eigenmodes of the non hermitian effective Hamiltonian (94). Fig. 23 clearly shows that BICs at $\Delta \phi \neq 0$ are decoupled from the first channel owing to twisting of the BIC modes by the rotation angle $\Delta \phi$.

7.2. Arbitrary $\Delta \phi$. Wave faucet.

Eq. (95) shows that the phase difference $\Delta\phi$ due to the rotation of the input waveguide brings an important contribution into interference between resonances. Fig. 24 vividly illustrates high sensitivity of the transmittance to the rotation angle $\Delta\phi$. As seen from Fig. 21 the eigenmode 012 crosses the eigenmodes ± 111 around L=5. Respectively the transmittance is basically given by the interference of these resonances in the vicinity of this crossing L=5, $\omega^2\approx 0.385$ (see parameters of the 1-th BIC in Table 5). According to Eq. (93) we have $W_{012;01}^L=-W_{012;01}^R$, $W_{\pm 111;01}^L=W_{\pm 111;01}^Re^{\mp i\Delta\phi}$. Therefore for the output waves interfering constructively we have to take $\Delta\phi=\pm\pi$, while the full destructive interference takes place at $\Delta\phi=0$. This simple consideration is in excellent agreement with numerics presented in Fig. 24 (a). Along the same line for channels 012 and ± 211 in the vicinity of L=3 we have from

Table 5: BICs at $\Delta \phi = \pi/4$. The waveguides with the unit radius are shifted relative to the axis of cylindrical resonator with radius R=3 by a distance $r_0=1.5$.

BIC	ω^2	L	mnl	a_{mnl}	$ a_{mnl} $
			012	-0.113+0.272i	0.294
1	0.385	5.065	111	-0.478(1-i)	0.675
			-111	0.675	0.675
			012	-0.261(1-i)	0.369
2	1.055	3.051	211	0.656i	0.656
			-211	0.656	0.656
			211	0.658i	0.658
3	1.0535	3.833	-211	0.658	0.658
			112	-0.237-0.098i	0.256
			-112	-0.098-0.237i	0.256
			211	-0.505	0.505
4	1.065	3.869	-211	0.505	0.505
			112	-0.455-0.189i	0.493
			-112	0.189+0.455i	0.493

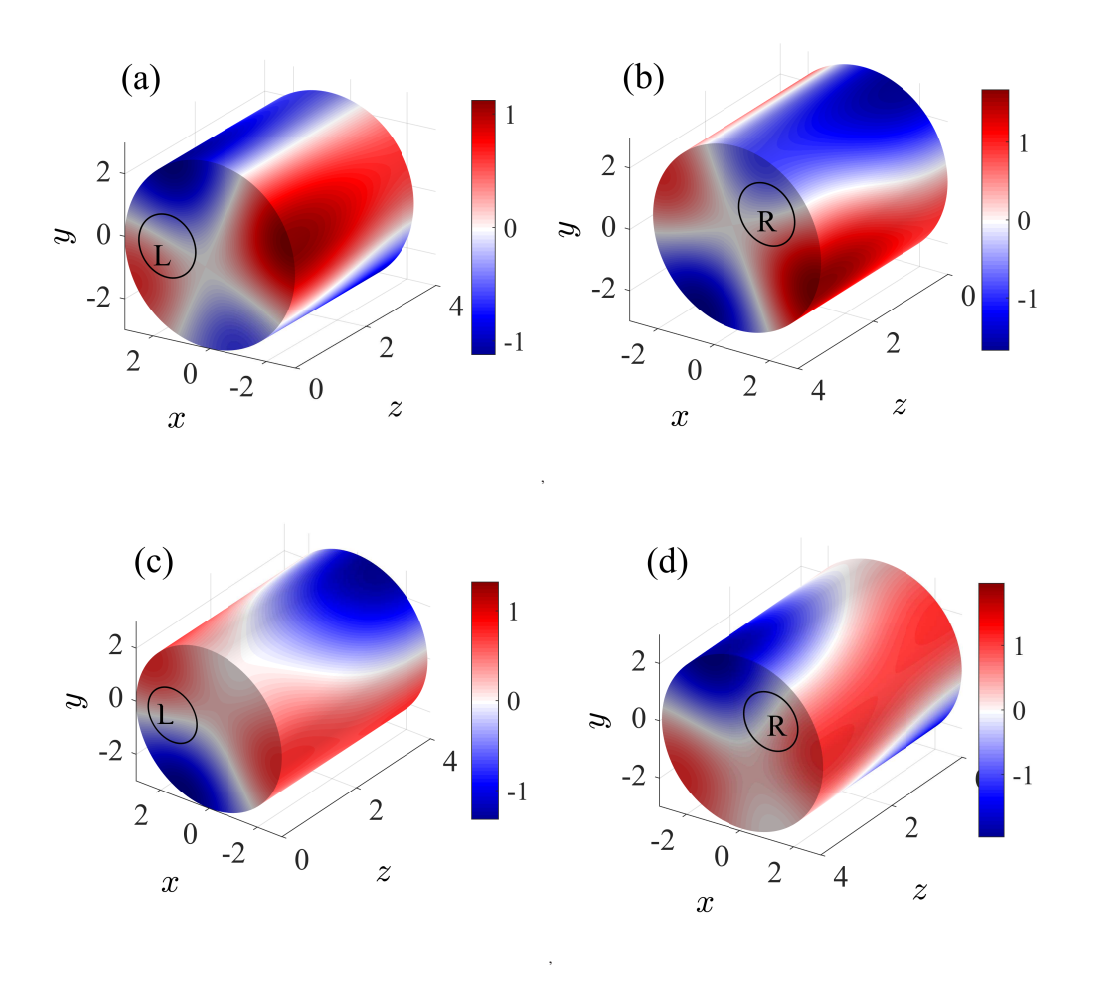


Figure 23: Patterns of BIC 3 shown from the left (a) and right (b) sides of the resonator and BIC 4 shown from the left (c) and right (d) sides of resonator on the surface of the waveguide at $\Delta \phi = \pi/4$.

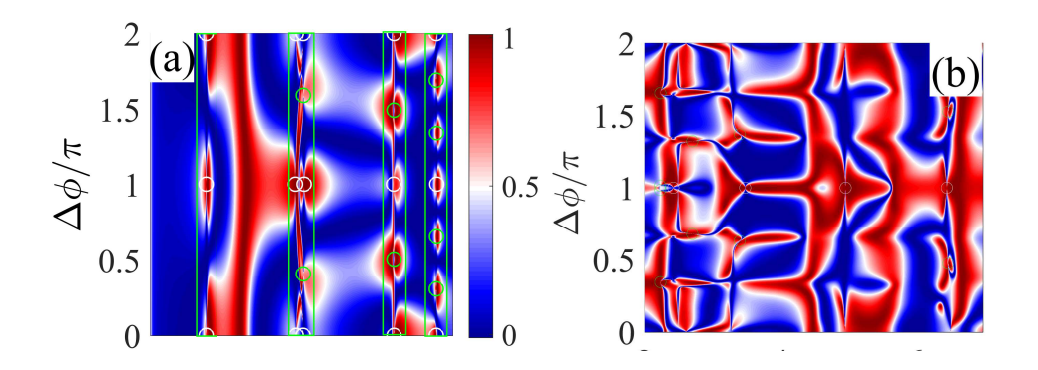


Figure 2 rotation angle at

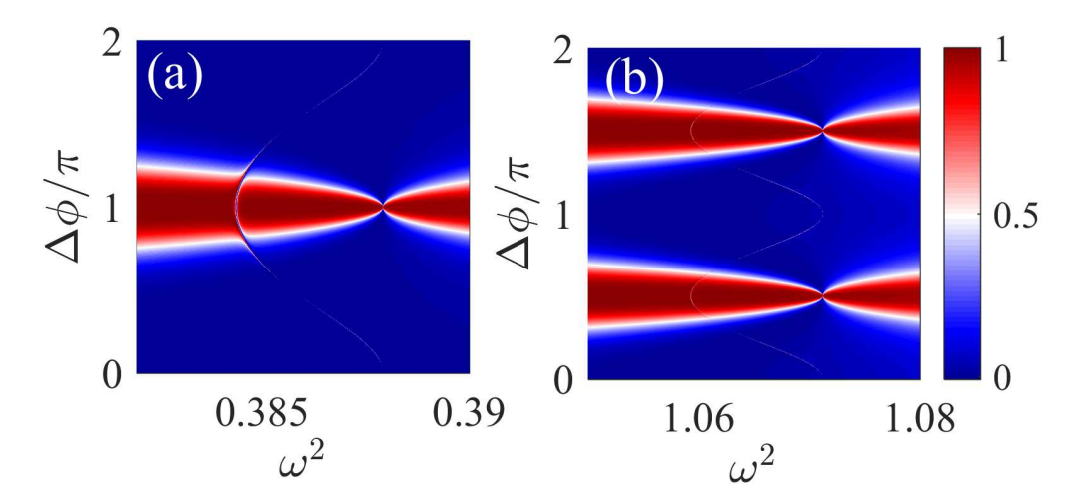


Figure 25: Transmittance vs the frequency and rotation angle in the vicinity of crossing of the modes (a) 012 and ± 111 at L=5, (b) 012 and ± 211 at L=3, and (c) ± 112 and ± 211 , L=4.

Eq. (93) $W^{\rm L}_{012;01} = -W^{\rm R}_{012;01}, W^{\rm L}_{\pm 211;01} = W^{\rm R}_{\pm 111;01} e^{\mp 2i\Delta\phi}$ to open wave flux through the resonator at $\Delta\phi = \pi/2, 3\pi/2$. That conclusion fully agrees with the transmittance shown in Fig. 24 (b). Thus, the rotation of the input waveguide strongly tunes Fano resonance [107]. In particular there can be a collapse of Fano resonance when the transmission zero approaches to the transmission maximum that is the signature of BICs (see the section 3).

Fig. 26 evidences that the rotation angle $\Delta\phi=\pi/4$ is not unique for BICs to occur. In fact, we will show below analytically that there is whole line $L=f(\Delta\phi)$ of BICs. Among them we select four BICs shown in Fig. 27. Let us consider the 1-th BIC from Table 6 whose azimuthal dependence is given by $\cos[3(\phi-\Delta\phi/2)]$. In order to decouple this BIC from the right waveguide at $\Delta\phi=0$ the nodal line of the BIC mode has to be positioned at $\phi=0$ that gives us the equation $\frac{3}{2}\Delta\phi=\frac{\pi}{2}$, i.e., $\Delta\phi=\frac{\pi}{3}$. Therefore the BIC mode is $\cos[3(\phi-\pi/6)]$ which equals zero at $\phi=0$. The left waveguide is rotated by the angle $\pi/3$ for which the BIC mode is decoupled from the left waveguide too. Numerically according to Table 6 we have $\Delta\phi=0.308\pi$ which is close to $\pi/3$. The small difference is a contribution of the evanescent modes. Similarly, for the 2-th BIC we obtain $\cos[4(\phi-\Delta\phi/2)]$ that gives us $\Delta\phi=\pi/4$ which is close to numerical result $\Delta\phi=0.235\pi$ given in Table 6. For the 4-th BIC we obtain that $\Delta\phi=\pi/2$ that also well agrees with Table 6. The most interesting is the 3-th BIC which is superposed of two modes $\cos[2(\phi-\Delta\phi/2)]$ and $\cos[(\phi+\Delta\phi/2)]$. As the result the BIC mode is twisted as shown in Figs. 23 and 27 (b) and (d).

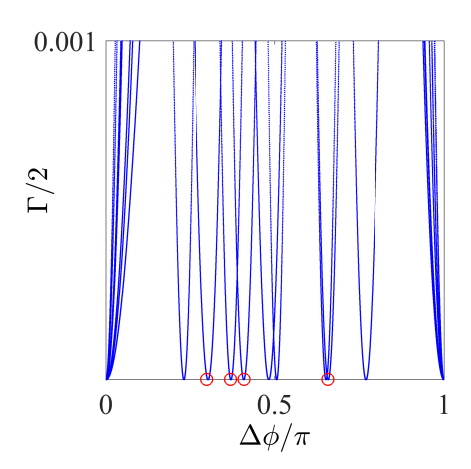


Figure 26: Evolution of resonant widths under waveguide rotation at L = 4.

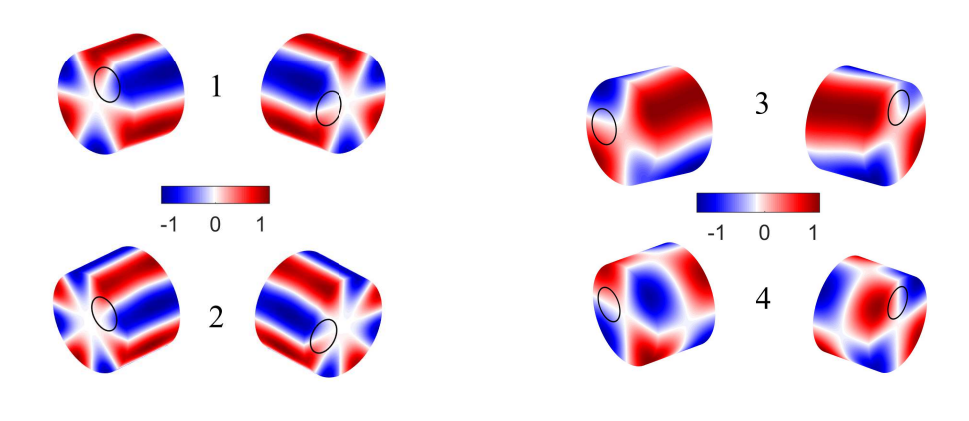


Figure 27: Patterns of BICs marked by open circles in Fig. 12 and listed in Table 6 on the surface of the resonator at L = 4: 1–4. Open circles show where the left and right waveguides are attached to the resonator.

7.3. CMT theory of twisted BICs

In the vicinity of crossings of eigenlevels of closed cylindrical resonator highlighted by green frames in Fig. 21 (a) it is reasonable to truncate the effective Hamiltonian (94) by only those modes which participate in crossing similar to the two-level description in section 6. The only difference is that, at least, three modes participate in degeneracy in the present case. For example, let consider the case when the eigenlevel $\omega_{012}^2 = \pi^2/L^2$ crosses with the double degenerate eigenlevel $\omega_{111}^2 = \mu_{11}^2/R^2$ shown in Fig. 28 (a) by dash lines. The coupling matrix elements of the eigenmodes with the first propagating mode p=0, q=1 (see Table 4) of the right waveguide according to Eqs. (86), (89) and (91) equal

$$W_{mnl;01}^{L} = (w_0 \ w_1 \ w_1), w_0 = W_{012;01}^{L} = \frac{1}{3} \sqrt{\frac{2}{L}},$$

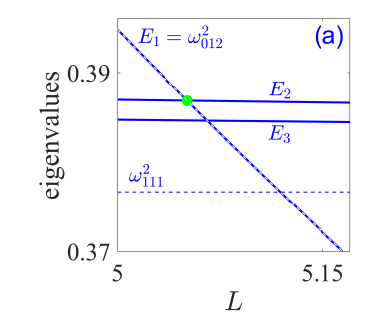
$$w_1 = W_{\pm 111;01}^{L} = 0.269 \sqrt{\frac{1}{L}}$$
(98)

for the given radius of the resonator. We also take into account the coupling with the first evanescent modes $p = \pm 1, q = 1$ of the waveguide (see Table 4)

$$W_{mnl;11}^{L} = (0 \ v_1 \ v_2), \ W_{mnl;-11}^{L} = (0 \ v_2 \ v_1),$$

$$v_1 = W_{012;11}^{L} = 0.1141 \sqrt{\frac{1}{L}}, \ v_2 = W_{\pm 111;11}^{L} = -0.0141 \sqrt{\frac{1}{L}}.$$
(99)

Table 6: BICs at $L = 4$.					
BIC	$\Delta\phi/\pi$	ω^2	mnl	a_{mnl}	
1	0.308	1.9868	311	0.7056	
			-311	$0.7056e^{-3i\Delta\phi}$	
2	0.2351	3.17304	411	0.705	
			-411	$0.705e^{4\mathrm{i}\Delta\phi}$	
3	0.4171	1.05688	211	0.6898	
			-211	$-0.6898e^{-2i\Delta\phi}$	
			121	0.0933+0.1215i	
			-121	$a_{121}e^{\mathrm{i}\Delta\phi}$	
4	0.5055	1.68872	211	0.7043	
			-211	$0.7043e^{-2i\Delta\phi}$	



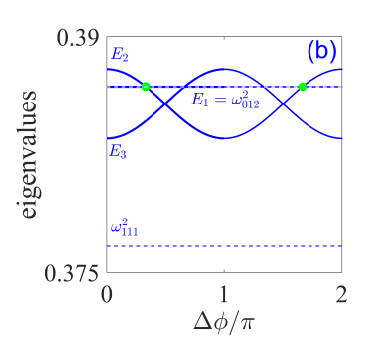


Figure 28: The eigenvalues ω_{012}^2 and ω_{111}^2 of the closed resonator are shown by dash lines while the eigenlevels (104) shifted by evanescent modes are shown by solid lines. (a) The eigenvalues (104) vs the resonator length at $\phi = \pi/3$ and (b) vs rotation angle at L = 5.0512.

Because of the phase difference between the coupling matrix elements for left and right waveguides we immediately obtain

$$\begin{split} W^{R}_{mnl;01} &= (-w_0 \ w_1 e^{i\Delta\phi} \ w_1 e^{-i\Delta\phi}), \\ W^{R}_{mnl;11} &= (0 \ v_2 e^{i\Delta\phi} \ v_1 e^{-i\Delta\phi}), \\ W^{R}_{mnl:-11} &= (0 \ v_1 e^{i\Delta\phi} \ v_2 e^{-i\Delta\phi}). \end{split} \tag{100}$$

The contribution of the higher evanescent modes shown in Table 4 is negligible. For open channel p=0, q=1 the wave number $q_{01}=\omega$ while for the next closed channel $p=\pm 1, q=1$ the wave number $k_{11}=iq_{11}, q_{11}=\sqrt{\mu_{11}^2-\omega^2}$ is imaginary. Then the truncated effective Hamiltonian (2) can be rewritten as follows

$$\widehat{H}_{eff} = \widehat{H}_R + q_{11} \sum_{C = L, R} \sum_{p = \pm 1} \widehat{W}_{p = \pm 1, 1}^C \{\widehat{W}_{p = \pm 1, 1}^C\}^{\dagger} - i\omega \sum_{C = L, R} \widehat{W}_{01}^C \{\widehat{W}_{01}^C\}^{\dagger} = \widehat{\widetilde{H}}_R - i\omega \widehat{\Gamma},$$
(101)

where the Hermitian term

$$\widehat{\widetilde{H}}_{R} = \begin{pmatrix}
\omega_{012}^{2} & 0 & 0 \\
0 & \omega_{111}^{2} + 2q_{11}(v_{1}^{2} + v_{2}^{2}) & 2q_{11}v_{1}v_{2}(1 + e^{-2i\Delta\phi}) \\
0 & 2q_{11}v_{1}v_{2}(1 + e^{2i\Delta\phi}) & \omega_{111}^{2} + 2q_{11}(v_{1}^{2} + v_{2}^{2})
\end{pmatrix}$$
(102)

is the Hamiltonian of the resonator coupled to the evanescent modes. The anti-Hermitian part takes the following form

$$\widehat{\Gamma} = \begin{pmatrix} 2w_0^2 & w_0 w_1 (1 - e^{i\Delta\phi}) & w_0 w_1 (1 - e^{-i\Delta\phi}) \\ w_0 w_1 (1 - e^{-i\Delta\phi}) & 2w_1^2 & w_1^2 (1 + e^{-2i\Delta\phi}) \\ w_0 w_1 (1 - e^{i\Delta\phi}) & w_1^2 (1 + e^{2i\Delta\phi}) & 2w_1^2 \end{pmatrix}.$$
(103)

The eigenvalues of the Hermitian part of the Hamiltonian (102) can be easily found as

$$E_1 = \omega_{012}^2, E_{2,3} = \omega_{111}^2 + 2q_{11}[v_1^2 + v_2^2 \pm 2v_1v_2\cos\Delta\phi]. \tag{104}$$

Thus the evanescent modes of the waveguides non-coaxially attached to the cylindrical resonator lift the degeneracy of eigenmodes ± 111 as shown in Fig. 28 by solid lines. The degeneracy is restored for $\Delta \phi = \pi/2, 3\pi/2$. The corresponding eigenmodes of the Hamiltonian (102) are the following

$$\mathbf{X}_1 = \begin{pmatrix} 1 \\ 0 \\ 0 \end{pmatrix}, \mathbf{X}_2 = \frac{1}{\sqrt{2}} \begin{pmatrix} 0 \\ -e^{-i\Delta\phi} \\ 1 \end{pmatrix}, \mathbf{X}_3 = \frac{1}{\sqrt{2}} \begin{pmatrix} 0 \\ e^{-i\Delta\phi} \\ 1 \end{pmatrix}. \tag{105}$$

Next, let us consider the BIC in the truncated version (101). The point of the BIC can be easily diagnosed by zero resonant width as shown in Fig. 29. For $\Delta \phi = \pi/4$ the BIC occurs at $L = L_c = 5.0512$ marked by closed green circle in Fig. 29 (a). Respectively at $L = L_c$ the BIC occurs at $\Delta \phi = \pi/4$ and $\Delta \phi = 2\pi - \pi/4$. These points are seen in zoomed insert in Fig. 29 (b).

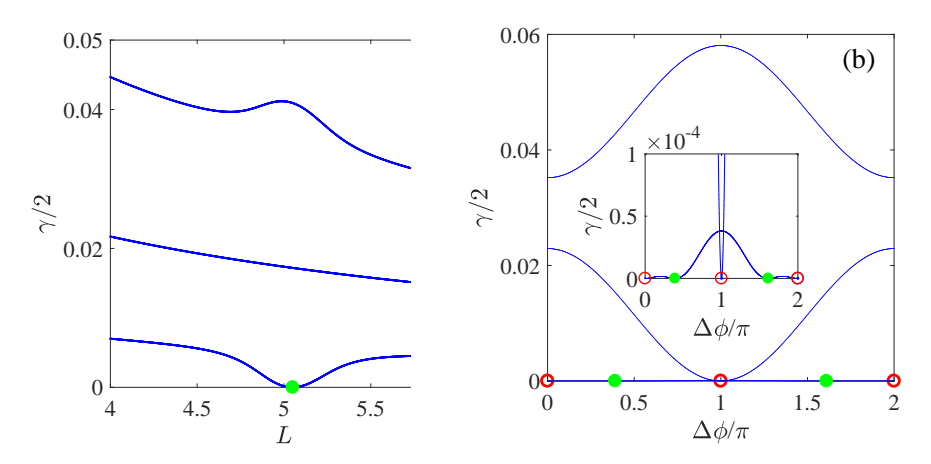


Figure 29: The resonant width vs (a) the resonator length at $\Delta \phi = \pi/4$ and (b) rotation angle at L = 5.0512. Open circles show the symmetry protected BICs, closed circles the FW BICs.

For $\Delta \phi = 0$ both continua of left and right waveguides coincide to result in the symmetry protected BIC superposed of degenerate eigenmodes of the closed resonator ψ_{111} and ψ_{-111} to be in the following form

$$\psi_{\rm BSC}(r,\phi,z) = AJ_1(\mu_{11}r)\sin(\pi z/L)\sin\phi \tag{106}$$

which always has zero coupling with the propagation mode $\psi_{01}(\rho, \alpha, z)$ shown in Table 4. As seen from Eq. (106) this conclusion also holds true for $\Delta \phi = \pi$. These BICs is trivial symmetry protected ones for arbitrary resonator length.

As soon as $\Delta\phi\neq0$ the continua become different to destroy the symmetry protected BICs. It could be expected that in the case of two waveguides the point of threefold degeneracy where the ω_{012} crosses the double degenerate ω_{111} as shown in Fig. 28 (a) is a BIC point in accordance with the above consideration. However the BIC point where the resonant width turns to zero (see Fig. 29) does not coincide with this point. The computation on the basis of full basis effective Hamiltonian gives the same result. In fact, the evanescent modes split the eigenvalues (104). Respectively the point of threefold degeneracy $\omega_{111}^2 = \omega_{012}^2(L)$ splits into two double degenerate points $E_1(L) = E_2(L, \Delta\phi)$ and $E_1(L) = E_3(L, \Delta\phi)$. As shown in Fig. 28 (a) the first case exactly corresponds to the BIC point but not the second case.

In the first case we can superpose the eigenmodes (105) as $a\mathbf{X}_1 + b\mathbf{X}_2$ and require zero coupling of this superposed mode with the left waveguide

$$aw_0 + \frac{b}{\sqrt{2}}w_1(1 - e^{-i\Delta\phi}) = 0 \tag{107}$$

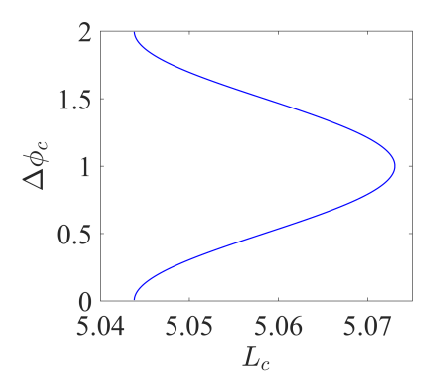


Figure 30: Line of the BICs in the parametric space of the resonator length and rotation angle $\Delta\phi$.

according to Eqs. (98) and (105). It is easy to show that the coupling with the phase shifted continuum of the left waveguide takes the *same* form as Eq. (107). Thus, the BIC has the following form

$$\psi_{\text{BSC}} = w_1 (1 - e^{-i\Delta\phi}) \psi_{012} + w_0 (e^{-i\Delta\phi} \psi_{111} - \psi_{-111}). \tag{108}$$

Substituting eigenmodes (89) into Eq. (108) we obtain

$$\psi_{\rm BSC} = 2ie^{-i\Delta\phi/2} [w_1 \sin(\Delta\phi/2)\psi_{01}(r)\psi_2(z) + w_0 \sin(\phi - \Delta\phi/2)\psi_{11}(r)\psi_1(z)]. \tag{109}$$

The BIC point is given by the equation $E_1(L) = E_2(L, \Delta \phi)$ which gives rise to a line of the BSC in the parametric space L and $\Delta \phi$ shown in Fig. 30.

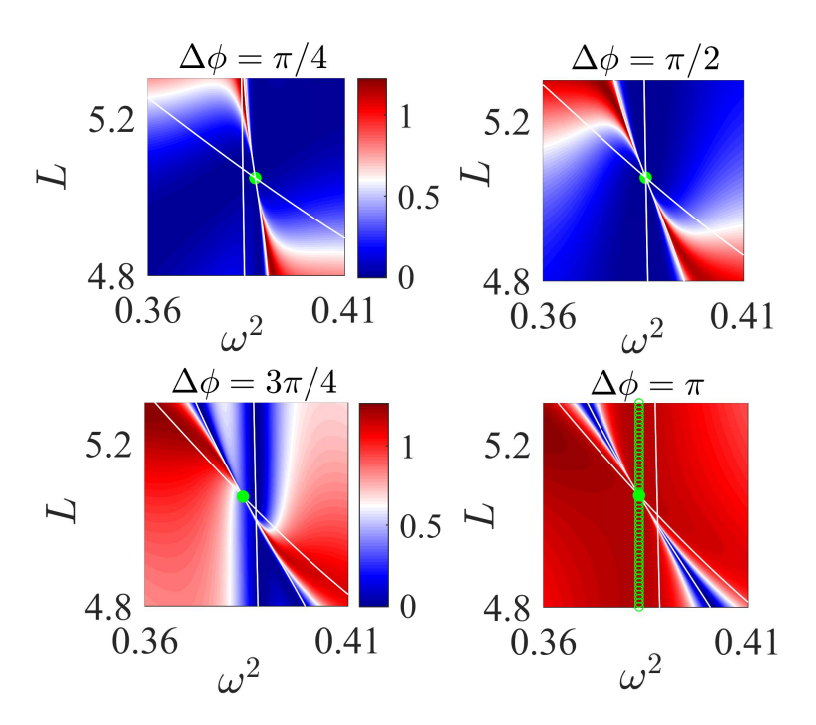


Figure 31: (a) Transmittance vs frequency and resonator length at four fixed rotation angles. Solid green lines show the resonances defined by real part of the complex eigenvalues of the effective Hamiltonian (101). Closed circles mark the BSCs which exactly correspond to points of degeneracy of the eigenlevels (104).

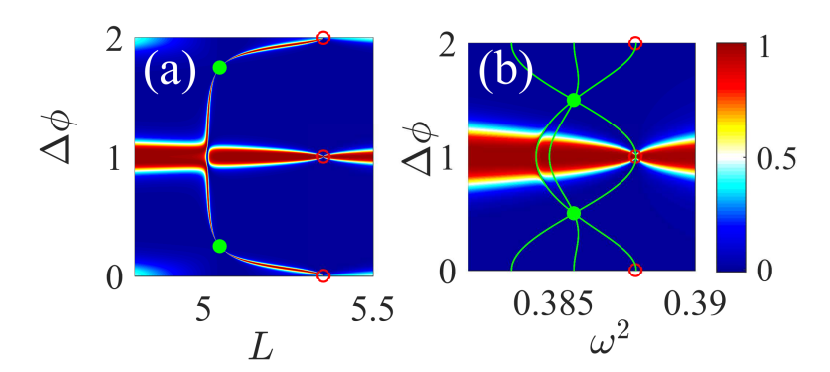


Figure 32: (a) Transmittance vs the resonator length and rotation angle for the frequency tuned onto the frequency of the BIC $\omega_c^2 = 0.388$. (b) Transmittance vs the frequency and rotation angle for the length tuned onto the BIC length $L_c = 5.048$. Closed circles mark BIC 1 resulted by crossing of eigenlevels (104) ω_{012}^2 and ω_{pm112}^2 , open circles mark the symmetry protected BICs (106).

Thus, the have shown occurrence of the BICs embedded into two continua which differ by phase in the point of twofold degeneracy. It is important to lay stress that this degeneracy refers to the eigenlevels of the Hamiltonian (102) of the cylindrical resonator modified by evanescent modes of attached waveguides. This is necessary condition for existence of BIC but not sufficient. Indeed let us consider the another point of degeneracy $E_1 = E_3$ (see Fig. 28 (a)). At this point we adjust the superposition $a\mathbf{X}_1 + b\mathbf{X}_3$ for cancellation of the coupling with both continua. The analogue of Eq. (107) takes the following form

$$\pm aw_0 + \frac{b}{\sqrt{2}}w_1(1 + e^{i\Delta\phi})w_1 = 0. \tag{110}$$

These equations can not be fulfilled simultaneously to forbid this degeneracy point as the BIC point. By the use of Eq. (95) and truncated effective Hamiltonian (101) we calculated the transmittance with the results presented in Fig. 31. Comparison to Fig. 21 (b) and (c) shows that all features of the transmittance can be well reproduced in the vicinity of the BICs by the use of truncated basis.

One can also see from Figs. 31 and 32 that the resonant features follow the real parts of the complex eigenvalues of the effective non-Hermitian Hamiltonian (101) when $\Delta\phi\neq0$. Fig. 32 shows fine features of the transmittance vs two parameters for the third parameter exactly tuned to the BIC. Fig. 32 (a) demonstrates a Fano resonance collapse in the parametric space of length and rotation angle at the BIC point $L_c=5.048$ and $\Delta\phi_c=\pi/4$ with the frequency exactly tuned to the BIC $\omega_c=0.3873$. Fig. 32 (b) shows the transmittance vs the frequency and the rotation angle for the length of the resonator tuned to the BIC length $L_c=5.0584$. Fig. 32 (a) and (b) shows that the resonator is blocked when $\Delta\phi=0$ and open when $\Delta\phi=\pi$. We skip here the case when the mode ± 112 crosses the mode ± 211 and refer the reader to the book chapter [108]. In spite of that the truncated effective Hamiltonian includes four states still this case allows analytical treatment of BICs.

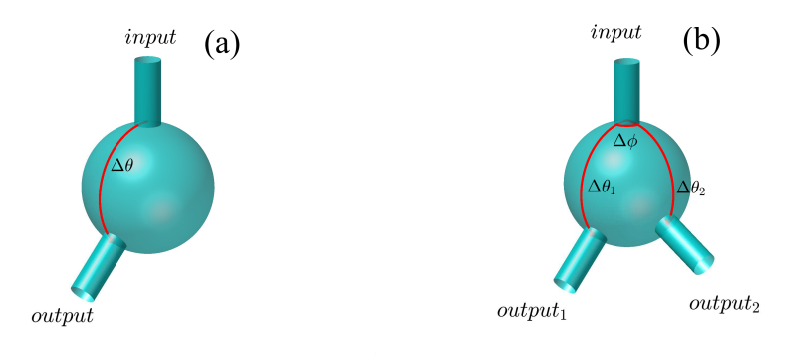


Figure 33: Spherical cavity of radius R with two (a) and (b) three attached cylindrical waveguides of the same radii r.

8. Spherical cavity

In this section we consider the FW BICs which exist only due to a contribution of evanescent modes of waveguides. Such an example is open spherical cavity shown in Fig. 33 which presents the system consisted of two subsystems with incompatible symmetries. The continua obey the cylindrical symmetry while the resonator does the spherical symmetry. Integrable spherical cavity has the only scale to vary the sphere radius R, which only scales the eigenvalues by the factor $\frac{1}{R^2}$. The eigenmodes are spherical functions which are 2l + 1-fold degenerated, where l is the orbital index. Let us attach two cylindrical waveguides as shown in Fig. 33 (a) that fully removes this degeneracy. Therefore it seems that the FW mechanism for the BICs due to an avoided crossing can not be applied here. The continua of the waveguides in the form of propagating Bessel modes transform the discrete eigenfrequencies of the closed cavity into the complex resonant frequencies whose positions depend on overlapping of the spherical functions with the Bessel modes. In turn, if the waveguides are angled by $\theta \neq \pi$ variation over that angle can give rise to avoided crossings of resonant modes with different *l* to result in the FW BICs.

In order to demonstrate this effect we use the coupled mode theory with the Neumann boundary conditions applicable for transmission of acoustic or EM waves with TM polarization [71]. It is easy to find a solution of the Helmholtz equation in spherical coordinates, so the eigenfunctions of a spherical cavity are the following

$$\Psi_{lmn} = \Psi_{ln}(r)Y_{lm}(\theta, \phi) \tag{111}$$

$$\Psi_{lmn} = \Psi_{ln}(r) Y_{lm}(\theta, \phi)$$

$$\Psi_{n}(r) = \frac{1}{R_{s}^{3/2}} \sqrt{\frac{2}{\kappa_{l+1/2,n}^{2} - n(n+1)}} \frac{\kappa_{l+1/2,n}}{J_{l+1/2}(\kappa_{l+1/2,n})} J_{l+1/2}(\frac{\kappa_{l+1/2,n}r}{R})$$

$$Y_{lm}(\theta, \phi) = \sqrt{\frac{(2l+1)(l-m)!}{4\pi(l+m)!}} P_{lm}(\cos \theta) \exp(m\phi)$$
(113)

$$Y_{lm}(\theta, \phi) = \sqrt{\frac{(2l+1)(l-m)!}{4\pi(l+m)!}} P_{lm}(\cos \theta) \exp(m\phi)$$
 (113)

where r, θ, ϕ are the spherical coordinates, R is the spherical cavity radius, Y_{lm} are the spherical harmonics, $P_{lm}(\cos\theta)$ are the associated Legendre polynomials, $J_{l+1/2}$ are the Bessel functions, $\kappa_{l+1/2,n}$ are the roots of the equation $\frac{dJ_{l+1/2,n}(\frac{\kappa_{l+1/2,n}r}{R_s})}{dr}\Big|_{r=R_s}$ Respective eigenfrequencies of the closed spherical resonator are given

$$\omega_{nl}^2 = \kappa_{l+1/2,n}^2 / R^2, \tag{114}$$

which are 2l + 1-fold degenerate over the azimuthal index -l < m < l. All the quantities are dimensionless and expressed in terms of the cylindrical waveguides radius a. The dimensionless frequency ω is expressed through the dimensional one $\tilde{\omega}$ as follows: $\omega = \tilde{\omega}a/s$ in acoustics or $\omega = cka$, where s/c is the sound/light velocity.

The eigenfunctions of the cylindrical waveguides are:

$$\psi_{pq}^{(C)}(\rho, \alpha, z) = \psi_{pq}^{(C)}(\rho) \frac{1}{\sqrt{2\pi k_{pq}^{(C)}}} \exp(ip\alpha + ik_{pq}^{(C)}z),$$

$$\psi_{pq}^{(C)}(\rho) = \begin{cases}
\frac{\sqrt{2}}{aJ_0(\mu_{0q})} J_0(\frac{\mu_{0q}\rho}{a}), p = 0, \\
\sqrt{\frac{2}{\mu_{pq}^2 - p^2}} \frac{\mu_{pq}}{aJ_p(\mu_{pq})} J_p(\frac{\mu_{pq}\rho}{a}), p = 1, 2, 3, \dots,
\end{cases}$$
(115)

where ρ, α are the polar coordinates in the x0y-plane in the waveguides reference system, $J_p(x)$ are the cylindrical Bessel functions of the first kind, μ_{pq} is the q-th root of equation $\frac{dJ_p(\mu_{pq}\rho)}{d\rho}\Big|_{\rho=a}=0$ imposed by the Neumann boundary condition on the walls of sound hard cylindrical waveguide, C enumerates input and output waveguides, $k_{pq}^{(C)}$ is the wave number:

 $k_{pq}^{(C)} = \sqrt{\omega^2 - \mu_{pq}^2/a^2},$

In order to write the non-Hermitian effective Hamiltonian it is necessary to calculate the coupling coefficients between the modes propagating in the waveguides and the eigenmodes of the spherical cavity. For the waveguide connected to the pole of the resonator, the coupling matrix elements can be calculated as follows [71, 102]:

$$W_{lmn,pq} = \Psi_{ln}(r = R) \int_0^{2\pi} d\phi \int_0^1 \rho d\rho \psi_{pq}(\rho, \phi) Y_{lm}(\theta(\rho, \phi), \phi)$$
(117)

where ρ is the radius in the cylindrical reference frame, $\phi = \alpha$ is the azimuthal angle, θ is the polar angle in the spherical reference frame. To perform this integration one has to express the spherical coordinates in terms of the cylindrical ones which could be done by a simple mathematical transformation. We assume here that the integration is carried out over the circular interface between the waveguides and the cavity in the limit R >> 1. Then the integration interface can be approximated by flat circle.

The calculation of the coupling matrix elements for asymmetrically connected waveguides is a bit difficult. We assume that these waveguides are also connected to the pole of the spherical resonator and then rotate the cavity eigenfunctions which is physically equivalent to rotation of the waveguides. For that procedure we use the Wigner *D*-matrix:

$$D_{mb}^{l}(\alpha,\beta,\gamma) = exp(-ik\alpha)d_{mb}^{l}(\beta)exp(-im\gamma), \tag{118}$$

where α, β, γ are the Euler's angles and $d_{mk}^l(\beta)$ is the small Wigner matrix

$$d_{mk}^{l} = \sqrt{\frac{(l-m)!(l+m)!}{(l-k)!(l+k)!}} \sum_{s=max(0,k-m)}^{min(l-m,l+k)} (-1)^{m-k+s}$$

$${\binom{l+k}{s}} {\binom{l-k}{m-k+s}} \cos^{2l-m+k-2s} \left(\frac{\beta}{2}\right) \sin^{m-k+2s} \left(\frac{\beta}{2}\right)$$
(120)

$$\binom{l+k}{s}\binom{l-k}{m-k+s}\cos^{2l-m+k-2s}\left(\frac{\beta}{2}\right)\sin^{m-k+2s}\left(\frac{\beta}{2}\right) \tag{120}$$

Then the rotated spherical harmonic can be expressed through the non-rotated one as follows

$$\tilde{Y}_{m}^{l}(\theta,\phi) = \exp(-im\gamma) \sum_{k=-l}^{l} \exp(-ik\alpha) d_{mk}^{l}(\beta) Y_{k}^{l}(\theta',\alpha'), \tag{121}$$

and the coupling matrix elements of the asymmetrically connected waveguides are the following

$$\tilde{W}_{lmn,pq} = \exp(-im\gamma) \sum_{k=-l}^{l} \exp(-ik\alpha) d_{mk}^{l} W_{lkn,pq}$$
(122)

Next, we write the effective non-Hermitian Hamiltonian of the system, which is the result of projection of the entire Hilbert space of the system "waveguides + cavity" onto the spherical cavity subspace

$$H_{eff} = H_B - i \sum_{C} \sum_{pq} k_{pq}^{(C)} W_{pq}^{(C)} W_{pq}^{(C)\dagger}$$
(123)

where the last term is given by the coupling matrix elements (117). Then the transmission coefficients from the channel pq of the waveguide (C) to the channel p'q' of the waveguide (C') are given by the following equations [71, 102]:

$$t_{pq;p'q'}^{(CC')} = 2i\sqrt{k_{pq}^{(C)}k_{p'q'}^{(C')}} \sum_{lmn} \sum_{l'm'n'} W_{lmn;pq}^{(C)} \frac{1}{\omega^2 - H_{eff}} W_{l'm'n';p'q'}^{(C')*},$$
(124)

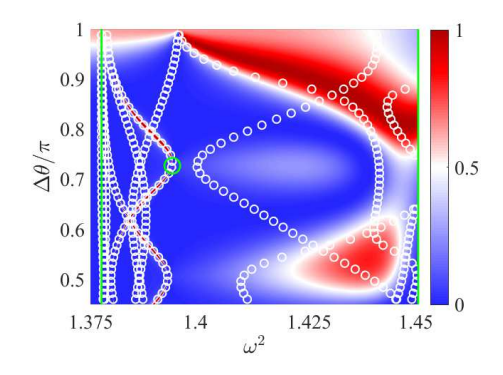


Figure 34: Transmittance of the spherical resonator vs the frequency of injected wave and displacement angle of the second waveguide. Small open white circles show the real part of eigenfrequencies of open cavity vs the second waveguide displacement angle. Large open green circle indicates the BIC point with the collapse of Fano resonance.

8.1. Two waveguides

An attachment of waveguides lifts the 2l+1-fold degeneracy of the eigenvalues of the closed spherical cavity as demonstrated in the Fig. 34 where the real parts of the effective Hamiltonian (123) complex eigenvalues are plotted by small open circles versus the rotation angle $\Delta\theta$. One can see from Fig. 34 that rotation of the second waveguide relative to the first waveguide splits resonances. The more important is, however, that such a rotation gives rise to the avoided crossing of resonances with different orbital indices l and respectively to the FW BIC which is marked by large open circle. Fig. 34 also shows the transmittance versus the injected wave frequency and the second waveguide displacement angle $\Delta\theta$. One can see that the narrow resonant peaks follow to the resonant frequencies marked by open circles. The small resonant widths are result of normalization coefficients of the eigenmodes of the spherical cavity (115) proportional to $\frac{1}{R^{3/2}}$. As a result the coupling matrix elements (117) have the same factor and the resonant widths which are given by squared coupling matrix elements turn out to be proportional to $\frac{1}{R^3}$ while the distance between the eigenfrequencies of H_B are proportional to $\frac{1}{R^2}$. Therefore for $R \ll 1$ we have the case of weak coupling of the sphere with the waveguide continuum.

The collapse of the Fano resonance, i.e. coincidence of the unit and zero transmittance, is the signature of the BIC [17, 34]. Fig. 34 shows one of these events at which imaginary part of the complex eigenvalues of the non Hermitian effective Hamiltonian vanishes. A major part of the BICs in the case of two waveguides are symmetry protected. These SP BICs can be obtained by simple rotation of the eigenfunctions of closed spherical resonator in order to achieve orthogonality of the eigenfunction to the mode of waveguide. We do not show here the symmetry protected BICs which coincide with the rotated eigen mode of closed cavity by use of the Wigner D-matrix.

However Fig. 34 marks the FW BIC at point $\Delta\theta=0.7\pi$, $\omega=1.378$ by open green circle. Fig. 35 (a) shows the FW BIC wave function (the pressure field/magnetic field) on the resonator surface. One can from nodal lines on the surface on sphere the BIC mode is decoupled from the first continuum of the waveguide with indices p=0, q=1. The modal expansion of this FW BIC over the eigen modes of the closed spherical cavity $\Psi_n l(r) Y_{lm}(\theta, \phi)$ is shown in Fig. 35 (b). The eigenmodes with quantum numbers $l=4, m=\pm 1, n=1$ and $l=1, m=\pm 1, n=2$ contribute into the FW BIC. Thus, the FW BIC is the result of full destructive interference of resonant modes with different orbital indices, despite that the eigenmodes of the closed spherical cavity with different orbital momentum l have different frequencies (116).

8.2. Three waveguides

Although the position of the second waveguide relative to the first one at the pole of sphere is given by two angles in general, only the polar angle $\Delta\theta_1$ is physically relevant for resonances and, in particular, for the BICs. Introduction of the third waveguide as shown in Fig. 33 (b) substantially changes effects of the continua onto the resonances because of three relevant angles, two polar angles $\Delta\theta_1$ and $\Delta\theta_2$ and one azimuthal angle $\Delta\phi$. Figs. 36 and 37 show the transmittance versus the frequency of injected wave and rotation angles $\Delta\theta_2$ and $\Delta\phi$ of the third waveguide which evident importance of mutual orientations of the all three waveguides. The regions in which avoid

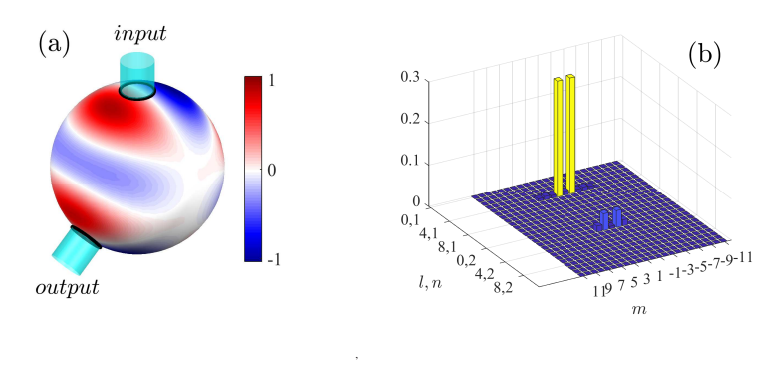


Figure 35: (a) The pressure field of the FW BIC at $\omega = 1.3937$ and $\Delta\theta = 0.727\pi$. (b) The modal decomposition of the BIC.

crossing phenomenon occurs, as well as the collapse of the Fano resonance, are highlighted by frames in Fig. 37. One can see that these phenomena take place irrespective to which waveguide goes wave.

The circle in the Figs. 36 and 37 marks the position of the FW BIC whose pattern in the form of surface pressure/magnetic field on surface of the resonator is shown in the Fig. 38 (a). The amplitudes a_{nlm} of superposition of spherical harmonics are chosen in so way that the nodal lines shown by white pass through the overlapping areas of waveguides with the spherical cavity. As a result the coupling constants of the FW BIC with the first propagating channel or continuum vanish.

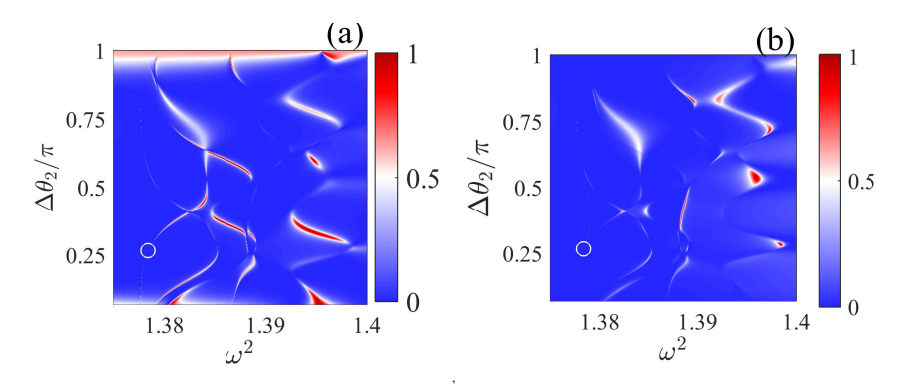


Figure 36: Transmittance between "input" and "output 1" (a) and "input" and "output 2" vs frequency and the displacement angle $\Delta\theta_2$ of the third waveguide for $\Delta\theta_1 = \pi/4$. The displacement angle of the second waveguide is $\Delta\theta_1 = 3\pi/4$. Crosses mark the FW BICs.

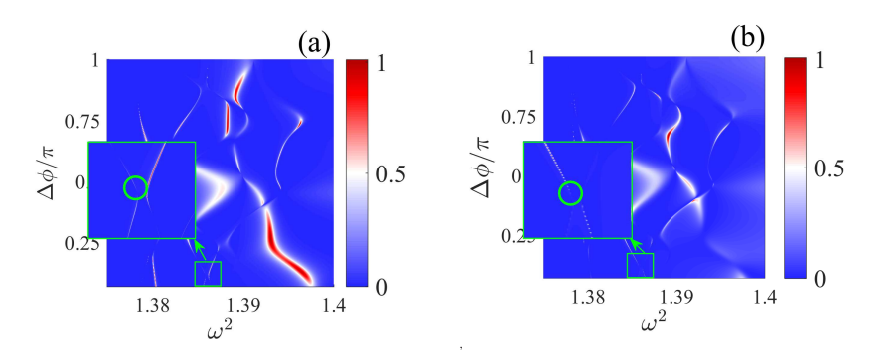


Figure 37: Transmittance between "input" and "output 1" (a) and "input" and "output 2" vs frequency and the displacement angle $\Delta\theta_2$ of the third waveguide for $\Delta\theta_1 = \sqrt{5}$.

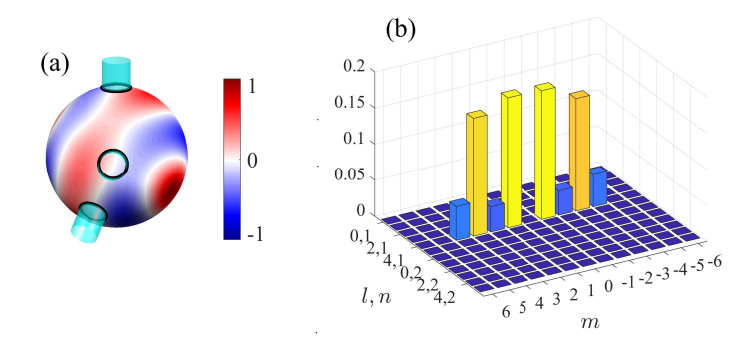


Figure 38: (a) The BIC pattern (pressure field) on surface of spherical cavity at the BIC point with $\omega=1.38575$, $\Delta\theta_1=\sqrt{5}$, $\Delta\theta_2=\sqrt{2}$ and $\Delta\phi=0.1222\pi$. (b) The modal decomposition of the BIC.

9. The Fabry-Perot mechanism of BICs in the system of two coupled resonators

If the double-barrier resonant structure had the infinitely high barriers the eigenmodes were localized between the barriers. For finite height of barriers these eigenmodes transform to the resonant modes with finite resonant widths defined by probability of tunnelling. Such a one-dimensional QM structure has one by one equivalency to the Fabry-Perot resonator (FPR) [109] and has no BICs as was discussed in section 4. Let us substitute the two-dimensional resonators instead of the barriers or mirrors in the FPR as presented in Fig. 39.

We start with the simplest case of 1d wire to which two off-side or off-channel cavities are attached as illustrated in Fig. 39 (a). The case of a single off-channel defect realizes the simplest way for Fano resonance due to interference of two wave paths, direct path over the wire and second path through the off-channel defect. As a result that gives rise to N transmission zeros at $\omega = \omega_n$, n = 1, 2, ..., N where N is the number of eigenfrequencies of the defect [70, 110]. Thus, the off-channel defects can serve as ideal Fano mirrors and support BICs provided that an integer of half-waves is placed between mirrors, i.e.,

$$\pi c n = \omega_n L \tag{125}$$

where *c* is the light velocity. Therefore, the underlying mechanism of the bound states in the FPR is (i) perfect reflections at mirrors and (ii) the integer number of the half waves between mirrors. This mechanism, exclusively transparent, for the bound states which we call as the Fabry-Perot (FP) BIC was applied to photonic crystal structure with one and two waveguides coupled with two single-mode cavities [40, 46, 47, 111, 112]. Technologically a tuning of eigenfrequencies of the off-channel defects can be performed by variation of their refractive index or size. However in Ref. [113] stable light trapping in the nonlinear Fabry-Perot resonator without necessity to tune the the distance between the off-channel defects was reported by implementation of an auxiliary nonlinear resonator.

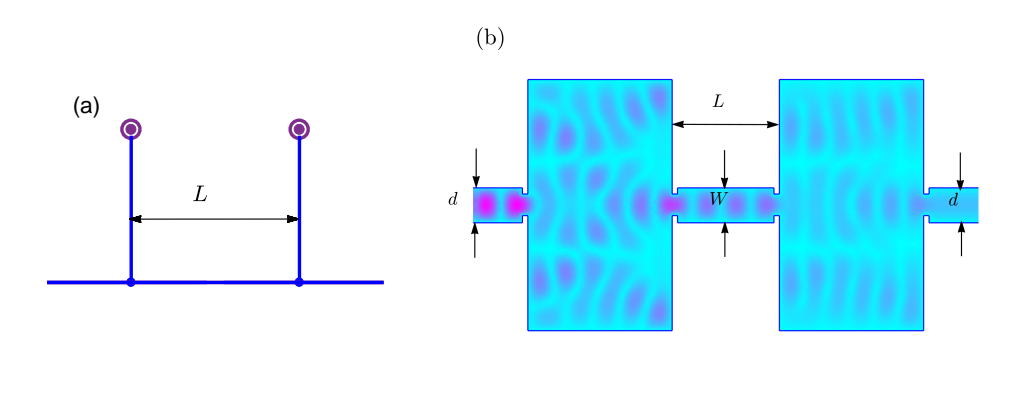


Figure 39: (a) 1d wire with two off-channel cavities. (b) 2d wire with two inserted identical resonators.

A different way is to implement two-dimensional cavities into waveguide as shown in Fig. 39 (b). Each resonator has transmission zeroes [114] at some frequencies to serve as Fabry-Perot mirrors. Therefore the total system consists of two cavities and a wire between them. In the simplest form the Hamiltonian of closed system has the following matrix structure

$$H_B = \begin{pmatrix} \epsilon_1 & 0 & u & 0 & 0 \\ 0 & \epsilon_2 & u & 0 & 0 \\ u & u & \epsilon_w & u & u \\ 0 & 0 & u & \epsilon_2 & 0 \\ 0 & 0 & u & 0 & \epsilon_1 \end{pmatrix}. \tag{126}$$

We can consider the eigenlevel of the wire ϵ_w is the parameter by which the system can be controlled.

The minimal rank of matrix (126) is five, so that let E_n and $|n\rangle$ with n=1,...,5 denote the five eigenlevels and eigenstates of (126). The amplitudes $\langle j=1,2|n\rangle$ describe the left resonator, $\langle j=3|n\rangle$ the waveguide, and $\langle j=4,5|n\rangle$ the right resonator. Two semi-infinite waveguides attached to the resonators provide continua and therefore transform the states of closed system into resonances which are described by the effective non-Hermitian Hamiltonian [70]

$$\langle m|H_{\text{eff}}|n\rangle = E_m \delta_{mn} - 2\pi i (V_L(m)V_L(n) + V_R(m)V_R(n))$$
(127)

with the coupling matrix elements

$$V_L(m) = v(k) \sum_{j=1,2} \langle j | m \rangle,$$

$$V_R(m) = v(k) \sum_{j=4,5} \langle j | m \rangle,$$
(128)

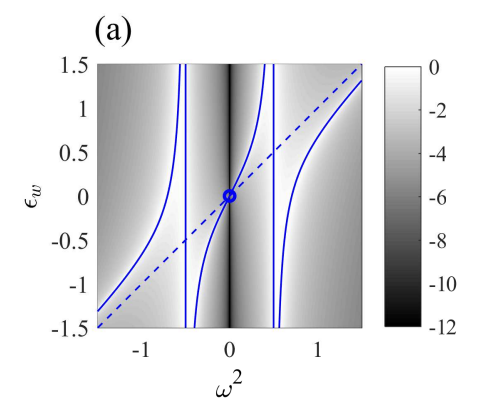
where the factors $\sqrt{\frac{k}{2\pi}}$ originated from the normalization of propagating states of 1d waveguides are absorbed by v(k).

The transmittance through the system given by Eq. (124) is shown in Fig. 40 (a) in Log scale in order to follow transmission zeros and resonances. Because of small coupling constant $v(k) = 0.5 \sqrt{\frac{k}{2\pi}}$ the transmittance demonstrates resonant behavior which follows the eigenlevels of the Hamiltonian (126) of closed system

$$E_{1.5} = \pm \eta, \quad E_2 = \epsilon_1, \quad E_3 = 0, \quad E_4 = \epsilon_2.$$
 (129)

The eigenvalues 2 and 4 of the effective Hamiltonian are independent of the wire's eigenvalue ε_w , while those of the other states depend on it. The eigenvalue 3, lying in the middle of the spectrum, crosses the transmission zero at

$$\epsilon_w = \epsilon_b = \frac{\epsilon_1 + \epsilon_2}{2} = 0. \tag{130}$$



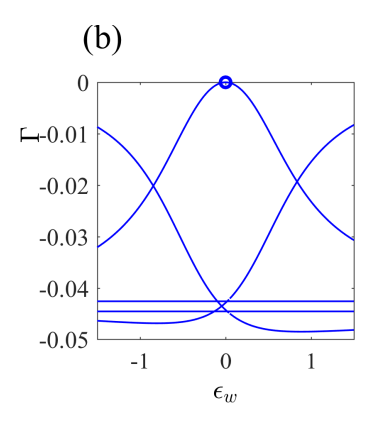


Figure 40: (a) The transmittance in Log scale through double resonator vs the frequency ϵ_W of wire and incident frequency $E = \omega^2$. (b) The resonant widths as dependent on ϵ_W at E = 0.5 at the following parameters of the system: $\epsilon_{1,2} = \pm 1/2$, v = 0.5, u = 1/4.

At this eigenvalue we observe the collapse of the Fano resonance that witnesses the BIC that fully agrees with turning to zero of resonant width as seen from Fig. 40 (b).

However still it is remaining a question where the BIC is localized, in the wire between the resonators or entirely in whole structure including resonators. It might be seemed that the latter answer taking into account that resonator provide large rooms for localization. Below by use of exact analytic equations we show that the first answer is correct, at least, in the present model case of 1d wire. The eigenstates of the Hamiltonian (126) are the following

$$\langle 1| = \frac{\sqrt{2}u}{\eta} \left(\frac{u}{\eta - \Delta \epsilon}, \frac{u}{\eta + \Delta \epsilon}, -1, \frac{u}{\eta + \Delta \epsilon}, \frac{u}{\eta - \Delta \epsilon} \right)$$

$$\langle 2| = \frac{1}{\sqrt{2}} (1, 0, 0, 0, -1)$$

$$\langle 3| = \frac{u}{\eta} \left(1, -1, \frac{\Delta \epsilon}{u}, -1, 1 \right)$$

$$\langle 4| = \frac{1}{\sqrt{2}} (0, 1, 0, -1, 0)$$

$$\langle 5| = \frac{\sqrt{2}u}{\eta} \left(\frac{u}{\eta + \Delta \epsilon}, \frac{u}{\eta - \Delta \epsilon}, 1, \frac{u}{\eta - \Delta \epsilon}, \frac{u}{\eta + \Delta \epsilon} \right)$$
(131)

where $\eta^2 = \Delta \epsilon^2 + 4u^2$, $\Delta \varepsilon = (\epsilon_2 - \epsilon_1)/2$. Substituting (131) into (128) we obtain

$$\langle m|V|E,C=L,R\rangle = v\sqrt{\frac{k}{8\pi}}(1\pm 1\frac{\Delta\epsilon}{\mu}\pm 1\ 1)$$
 (132)

for the elements of the coupling matrix. One can see that, under the condition (130), the wire decouples from the rest

of the system with zero imaginary part of the third eigenvalue of H_{eff} , i.e. the width of the third eigenstate vanishes at $\varepsilon_w = \varepsilon_b$.

In conclusion we present numerically computed transmittance through planar metallic double resonator connected by planar two-dimensional waveguide in Fig. 41. Total view of the double resonator connected to semi-infinite waveguide through diaphragms is shown in Fig. 39 (b). This figure also shows the scattering wave function. Fig.

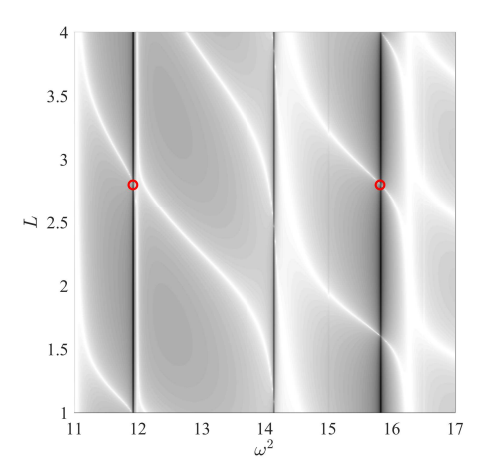


Figure 41: The transmittance in Log scale of the double resonator shown in Fig. 39 (b) versus frequency and length of the waveguide between the resonators. The bold open circles mark two points of BICs shown in the next Fig. 42.

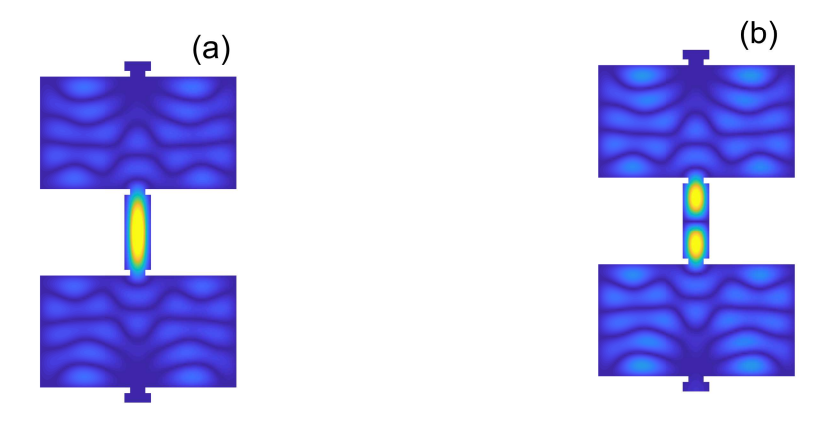


Figure 42: BICs at points marked by open circles in Fig. 41: (a) at $\omega^2 = 11.92$ and L = 2.8 and (b) $\omega^2 = 15.83$ and L = 2.83.

42 presents two patterns of the BICs which correspond to the Fabry-Perot resonances n = 1 (a) and n = 2 (b) in Eq. (125). Details of the Fabry-Perot BICs the reader can find in Refs. [43, 44]. Note that different scheme for the Fabry-Perot BICs was presented by Marinica *et al* in which arrays of dielectric cylinders play role of mirrors at the frequency of full reflection [46, 48].

10. Conclusions

The present review is addressed first of all to the Friedrich-Wintgen mechanism of localization of waves in the open electromagnetic (metallic) and acoustic cavities. The mechanism is based on full destructive interference of two resonant modes outgoing from the cavity. Although we presented the three-dimensional symmetrical cavities, cylindrical and spherical, in which BICs are result of destructive interference of more resonances. The cavities are

open by attachment of directional waveguides which provide well separated continua of propagating modes. Therefore such waveguide systems have the advantage of controlling the number of continua by crossing the cutoff frequencies. Throughout the review we almost entirely used two identical waveguides to have identical the continua of waveguides. Importantly, the open resonators are one of the best systems where the effective non-Hermitian Hamiltonian can be derived analytically with exact expressions for the coupling matrix. Moreover the identical waveguides can be attached to the resonant cavities of cylindrical or spherical shapes in such a way that the coupling matrices for the two waveguides differ by phase. That simple way to distinguish the continua gives us an additional parameter to control the wave transmission (wave faucet) and realize twisted BICs.

The evanescent modes with cutoffs above the BIC frequencies have also principal importance for the BICs: first due to the boundary conditions between localized BIC mode and evanescent modes the BICs exist and slightly stand out from the cavity. Because of absence of evanescent modes in one-dimensional wires there is no BICs in the cavity opened by attachment half-infinite wires. That is only true for the one-dimensional quantum wires or layered structures where TE and TM polarizations are separated. For the case of spinor fields transmission like one-dimensional electron transmission through the quantum dot we show that the FW BICs can occur due to the full destructive interference of resonances with opposite spins. The same idea can be applied to defect anisotropic layer where EM waves with TE and TM polarization can destructively interfere [97].

Second, the evanescent modes contribute into the Hamiltonian of the closed cavity similar to the Lamb shift in atomic physics. The coupling to evanescent modes shifts the BIC point from the point of degeneracy of the closed cavity. However, the most striking effect is that the FW BICs exist only owing to the evanescent modes as it was demonstrated in the open spherical cavity.

Although the FW mechanism of the BICs is the most generic and interesting we have reviewed also another mechanisms of the BICs. The second mechanism is vanishing of the coupling of some eigenmode of the cavity with the continuum that results in accidental BICs. As an example we considered the open chaotic Sinai billiard (rectangular resonator with hole inside) in which variation of the hole's diameter gives changes the coupling constants and finally to the accidental BICs.

There are no BICs in one-dimensional system except specially chosen long-range oscillating potentials by von Neumann and Wigner [1]. However that is truth only for scalar waves. For vectorial waves again the FW mechanism of BICs can be applied however as a result of full destructive interference of resonances corresponding to different components of the vectorial field [97].

Finally we have reviewed the Fabry-Perot mechanism for the BICs when the off-channel defects or two-dimensional cavities integrated into waveguide can serve as ideal mirrors due to transmission zeroes of the cavities.

One of the most remarkable results for BICs is their existence in photonic crystal systems embedded into the radiation continuum which has infinite number of continua because of dispersion equation $\omega = ck$. It may be seemed that there are not possible BICs embedded into the radiation continuum. Indeed rigorous theorem forbids BICs in finite dielectric structure [58]. However, if we take the infinite periodic PhC structures like 2d PhC surface, one-dimensional array of dielectric particles we obtain an analogue of diffraction lattices which are coupled with only discretized continua defined as the diffraction orders. That is physical expalantion for BIC in such infinite PhC structures [31, 60].

Here we skipped the majority of results on BICs in photonics for two reasons. First, this research direction is so rapidly developing and huge that it could hardly be put into a single review. We only included one example of BICs in one-dimensional photonic crystal holding the defect anisotropic layer in which the BICs are realized because of full destructive interference of resonance with TE and TM polarizations. The second reason is that the recent reviews have filled this gap [62–65] already.

Acknowledgments First of all I am grateful to Ingrid Rotter who introduced me to concept and machinery of non Hermitian Hamiltonian and with whom we first revealed the phenomenon of vanishing of resonant width. I would like express gratitude to my colleagues with whom I worked long time in the field of bound states in the continuum, Evgeny N. Bulgakov, Dmittrii N. Maksimov, Konstantin N. Pichugin, Artem A. Pilipchuk, and Alina Pilipchuk. I also had a lot of discussions with researches over all the world: Andrey A. Bogdanov, Yi Xu, Dezhuan Han, Egor Muliarov, Ivan Timofeev, Pavel Pankin, Evgeny Kamenetskii, Andrey Miroshnichenko, Yurii Kivshar, Kirill Koshelev, Ya Yan Lu, Evgeny Sherman. My special thanks to Monti Segev who initiated me to write this review.

The work was partially supported by Russian Foundation for Basic Research projects No. 19-02-00055.

References

- [1] J. von Neumann, E. P. Wigner, Über merkwürdige diskrete eigenwerte, Z. Physik 30 (1929) 465–467. doi:10.1007/978-3-662-02781-3√19.
- [2] F. Stillinger, D. Herrick, Bound states in the continuum, Phys. Rev. A 11 (2) (1975) 446-454. doi:10.1103/physreva.11.446.
- [3] J. U. Nöckel, Resonances in quantum-dot transport, Phys. Rev. B 46 (23) (1992) 15348-15356. doi:10.1103/physrevb.46.15348.
- [4] T. A. Weber, D. L. Pursey, Continuum bound states, Physical Review A 50 (1994) 4478–4487.
- [5] D. Pursey, T. Weber, Scattering from a shifted neumann-wigner potential, Physical Review A 52 (1995) 3932–3939.
- [6] L. S. Cederbaum, R. S. Friedman, V. M. Ryaboy, N. Moiseyev, Conical intersections and bound molecular states embedded in the continuum, Phys. Rev. Lett. 90 (2003) 013001. doi:10.1103/physrevlett.90.013001.
- [7] H. Friedrich, D. Wintgen, Interfering resonances and bound states in the continuum, Physical Review A 32 (6) (1985) 3231–3242. doi:10.1103/physreva.32.3231.
- [8] H. Feshbach, Unified theory of nuclear reactions, Annals of Physics 5 (1958) 357–390. doi:10.1016/0003-4916(58)90007-1.
 URL http://dx.doi.org/10.1016/0003-4916(58)90007-1
- [9] H. Feshbach, A unified theory of nuclear reactions. II, Annals of Physics 19 (2) (1962) 287-313. doi:10.1016/0003-4916(62)90221-x.
- [10] T. V. Shahbazyan, M. E. Raikh, Two-channel resonant tunneling, Physical Review B 49 (24) (1994) 17123–17129. doi:10.1103/physrevb.49.17123.
- [11] A. Magunov, I. Rotter, S. Strakhova, Laser-induced resonance trapping in atoms, J. Phys. B: At. Mol. Opt. Phys. 32 (1999) 1669–1684.
- [12] A. Volya, V. Zelevinsky, Non-hermitian effective hamiltonian and continuum shell model, Phys. Rev. C 67 (2003) 054322. doi:10.1103/physrevc.67.054322.
- [13] M. L. L. de Guevara, F. Claro, P. A. Orellana, Ghost fano resonance in a double quantum dot molecule attached to leads, Physical Review B 67 (19) (may 2003). doi:10.1103/physrevb.67.195335.
- [14] B. Wunsch, A. Chudnovskiy, Quasistates and their relation to the dicke effect in a mesoscopic ring coupled to a reservoir, Physical Review B 68 (2003) 245317. doi:10.1103/physrevb.68.245317.
- [15] M. Fedorov, N. Poluektov, Two-color interference stabilization of atoms, Phys. Rev. A 69 (2004) 033404. doi:10.1103/PhysRevA.69.033404.
- [16] I. Rotter, A. F. Sadreev, Zeros in single-channel transmission through double quantum dots, Physical Review E 71 (2005) 046204. doi:10.1103/physreve.71.046204.
- [17] A. F. Sadreev, E. N. Bulgakov, I. Rotter, Bound states in the continuum in open quantum billiards with a variable shape, Physical Review B 73 (23) (2006) 235342.
- [18] M. L. L. de Guevara, P. A. Orellana, Electronic transport through a parallel-coupled triple quantum dot molecule: Fano resonances and bound states in the continuum, Physical Review B 73 (2006) 205303. doi:10.1103/physrevb.73.205303.
- [19] B. Solís, M. L. de Guevara, P. Orellana, Friedel phase discontinuity and bound states in the continuum in quantum dot systems, Physics Letters A 372 (26) (2008) 4736–4739. doi:10.1016/j.physleta.2008.05.014.
- [20] J.-M. Jin, Theory and computation of electromagnetic fields, Wiley and A John Wiley & Sons, Inc., Publication, 2010.
- [21] T. Lepetit, B. Kanté, Controlling multipolar radiation with symmetries for electromagnetic bound states in the continuum, Physical Review B 90 (2014) 241103(R). doi:10.1103/physrevb.90.241103.
- [22] O. Olendski, L. Mikhailovska, Bound-state evolution in curved waveguides and quantum wires, Physical Review B 66 (2002) 035331. doi:10.1103/physrevb.66.035331.
- [23] G.Cattapan, P. Lotti, S-matrix poles close to thresholds in confined geometries, The Europ. Phys. Journal B 60 (2007) 181–185. doi:10.1140/epjb/e2007-00337-6.
- [24] G. Cattapan, P. Lotti, Fano resonances in stubbed quantum waveguides with impurities, The European Physical Journal B 60 (1) (2007) 51–60. doi:10.1140/epjb/e2007-00325-x.
- [25] M. Bolsterli, Continuity of phase shift at continuum bound state, Phys. Rev. 182 (1969) 1095–1096.
- [26] M. Robnik, A simple separable Hamiltonian having bound states in the continuum, J. Phys. A: Math. Gen. 19 (18) (1986) 3845–3848. doi:10.1088/0305-4470/19/18/029.
- [27] R. L. Schult, D. G. Ravenhall, H. W. Wyld, Quantum bound states in a classically unbound system of crossed wires, Phys. Rev. B 39 (8) (1989) 5476-5479. doi:10.1103/PhysRevB.39.5476.
- [28] N. Moiseyev, Suppression of feshbach resonance widths in two-dimensional waveguides and quantum dots: A lower bound for the number of bound states in the continuum, Phys. Rev. Lett. 102 (2009) 167404.
- [29] A. Pilipchuk, A. Sadreev, Accidental bound states in the continuum in an open sinai billiard, Physics Letters A 381 (7) (2017) 720–724. doi:10.1016/j.physleta.2016.11.022.
- [30] H. Friedrich, D. Wintgen, Physical realization of bound states in the continuum, Physical Review A 31 (6) (1985) 3964–3966.
- [31] Chia Wei Hsu, Bo Zhen, Jeongwon Lee, S. G. Johnson, J. D. Joannopoulos, M. Soljačić, Observation of trapped light within the radiation continuum, Nature 499 (2013) 188–191. doi:10.1038/nature12289.
- [32] E. N. Bulgakov, A. F. Sadreev, Bloch bound states in the radiation continuum in a periodic array of dielectric rods, Phys. Rev. A 90 (2014) 053801. doi:10.1103/physreva.90.053801.
- [33] J. A. Stratton, Electromagnetic theory, McGraw-Hill Book Company, Inc., 1941.
- [34] C. S. Kim, A. M. Satanin, Y. S. Joe, R. M. Cosby, Resonant tunneling in a quantum waveguide: Effect of a finite-size attractive impurity, Phys. Rev. B 60 (1999) 10962.
- [35] H. Sambe, Steady states and quasienergies of a quantum-mechanical system in an oscillating field, Phys. Rev. A 7 (1973) 2203–2213.
- [36] A. F. Sadreev, Feshbach projection formalism for transmission through a time-periodic potential, Physical Review E 86 (5) (2012) 056211.
- [37] S. Longhi, G. Valle, Dynamic reflectionless defects in tight-binding lattices, Physical Review B 84 (2011) 193105.
- [38] S. Longhi, G. Valle, Floquet bound states in the continuum, Scientific Reports 3:2219 (2013) 1-6.

- [39] G. Valle, S. Longhi, Floquet-hubbard bound states in the continuum, Physical Review B 89 (2014) 115118. doi:10.1103/PhysRevB.89.115118.
- [40] S. Fan, P. R. Villeneuve, J. D. Joannopoulos, M. J. Khan, C. Manolatou, H. A. Haus, Theoretical analysis of channel drop tunneling processes, Physical Review B 59 (24) (1999) 15882–15892.
- [41] W. Suh, Z. Wang, S. Fan, Temporal coupled-mode theory and the presence of non-orthogonal modes in lossless multimode cavities, IEEE Journal of Quantum Electronics 40 (10) (2004) 1511–1518. doi:10.1109/jqe.2004.834773.
- [42] I. Rotter, A. F. Sadreev, Influence of branch points in the complex plane on the transmission through double quantum dots, Physical Review E 69 (6) (2004) 066201.
- [43] A. Sadreev, E. Bulgakov, I. Rotter, Trapping of an electron in the transmission through two quantum dots coupled by wire, JETP Letters 82 (8) (2005) 556–561.
- [44] A. Sadreev, E. Bulgakov, I. Rotter, S-matrix formalism of transmission through two quantum billiards coupled by a waveguide, Journal of Physics A: Mathematical and General 38 (2005) 10647–10661. doi:10.1088/0305-4470/38/49/012.
- [45] G. Ordonez, K. Na, S. Kim, Bound states in the continuum in quantum-dot pairs, Physical Review A 73 (2006) 022113. doi:10.1103/physreva.73.022113.
- [46] D. C. Marinica, A. G. Borisov, S. V. Shabanov, Bound states in the continuum in photonics, Physical Review Letters 100 (18) (2008) 183902. doi:10.1103/physrevlett.100.183902. URL http://dx.doi.org/10.1103/PhysRevLett.100.183902
- [47] E. N. Bulgakov, A. F. Sadreev, Bound states in the continuum in photonic waveguides inspired by defects, Phys. Rev. B 78 (2008) 075105. doi:10.1103/PhysRevB.78.075105.
- [48] R. F. Ndangali, S. V. Shabanov, Electromagnetic bound states in the radiation continuum for periodic double arrays of subwavelength dielectric cylinders, Journal of Mathematical Physics 51 (10) (2010) 102901. doi:10.1063/1.3486358. URL http://dx.doi.org/10.1063/1.3486358
- [49] L. Li, H. Yin, Bound states in the continuum in double layer structures, Scientific Reports 6 (1) (2016) 26988. doi:10.1038/srep26988.
- [50] A. F. Sadreev, D. N. Maksimov, A. S. Pilipchuk, Gate controlled resonant widths in double-bend waveguides: bound states in the continuum, Journal of Physics: Condensed Matter 27 (2015) 295303. doi:10.1088/0953-8984/27/29/295303.
- [51] S. Hein, W. Koch, Acoustic resonances and trapped modes in pipes and tunnels, Journal of Fluid Mechanics 605 (2008) 401–428. doi:10.1017/s002211200800164x.
- [52] S. Hein, W. Koch, L. Nannen, Trapped modes and fano resonances in two-dimensional acoustical duct-cavity systems, J. Fluid Mech. 692 (2012) 257–287. doi:10.1017/jfm.2011.509.
- [53] V. Vargiamidis, V. Fessatidis, N. J. M. Horing, Electric-field effects on fano resonances and transmission phase through quantum wires, Journal of Applied Physics 106 (4) (2009) 043710. doi:10.1063/1.3204778.
- [54] K. D. Rowe, P. J. Siemens, Unusual quantum effects in scattering wavefunctions of two-dimensional cage potentials, Journal of Physics A: Mathematical and General 38 (45) (2005) 9821–9847. doi:10.1088/0305-4470/38/45/007.
- [55] E. Bulgakov, A. Sadreev, Formation of bound states in the continuum for a quantum dot with variable width, Phys. Rev. B 83 (2011) 235321. doi:10.1103/physrevb.83.235321.
- [56] F. Monticone, A. Alù, Embedded photonic eigenvalues in 3D nanostructures, Physical Review Letters 112 (21) (2014) 213903. doi:10.1103/physrevlett.112.213903.
- [57] M. G. Silveirinha, Trapping light in open plasmonic nanostructures, Physical Review A 89 (2) (2014) 023813. doi:10.1103/physreva.89.023813.
- [58] D.Colton, R.Kress, Inverse Acoustic and Electromagnetic Scattering Theory, 2nd Edition, Springer, Berlin, 1998.
- [59] Yang Yi, Peng Chao, Liang Yong, Li Zhengbin, S. Noda, Analytical perspective for bound states in the continuum in photonic crystal slabs, Physical Review Letters 113 (3) (2014) 037401. doi:10.1103/physrevlett.113.037401.
- [60] E. Bulgakov, A. Sadreev, Light trapping above the light cone in a one-dimensional array of dielectric spheres, Phys. Rev. A 92 (2015) 023816. doi:10.1103/physreva.92.023816.
- [61] E. N. Bulgakov, A. F. Sadreev, Bound states in the continuum with high orbital angular momentum in a dielectric rod with periodically modulated permittivity, Phys. Rev. A 96 (2017) 013841. doi:10.1103/physreva.96.013841.
- [62] Chia Wei Hsu, Bo Zhen, A. D. Stone, J. D. Joannopoulos, M. Soljačić, Bound states in the continuum, Nature Reviews Materials 1 (9) (2016) 16048. doi:10.1038/natrevmats.2016.48.
- [63] A. Krasnok, D. Baranov, H. Li, M.-A. Miri, F. Monticone, A. Alú, Anomalies in light scattering, Advances in Optics and Photonics 11 (4) (2019) 892–951. doi:10.1364/aop.11.000892.
- [64] K. Koshelev, G. Favraud, A. Bogdanov, Y. Kivshar, A. Fratalocchi, Nonradiating photonics with resonant dielectric nanostructures, Nanophotonics 8 (5) (2019) 725–745. doi:10.1515/nanoph-2019-0024.
- [65] Y. Peng, S. Liao, Bound states in continuum and zero-index metamaterials: A review (2020). arXiv:2007.01361v1.
- [66] I. Rotter, A continuum shell model for the open quantum mechanical nuclear system, Reports on Progress in Physics 54 (4) (1991) 635–682. doi:10.1088/0034-4885/54/4/003.
- [67] F. Dittes, The decay of quantum systems with a small number of open channels, Physics Reports 339 (4) (2000) 215–316. doi:10.1016/s0370-1573(00)00065-x.
- [68] M. P. J. Okołowicz, I. Rotter, Dynamics of quantum systems embedded in a continuum, Physical Reports 374 (2003) 271–383. doi:10.1016/S0370-1573(02)00366-6.
- [69] D. V. Savin, V. V. Sokolov, H.-J. Sommers, Is the concept of the non-hermitian effective hamiltonian relevant in the case of potential scattering?, Physical Review E 67 (2) (2003). doi:10.1103/physreve.67.026215.
- [70] A. Sadreev, I. Rotter, S-matrix theory for transmission through billiards in tight-binding approach, Journal of Physics A: Math. Gen. 36 (2003) 11413–11433. doi:10.1088/0305-4470/36/45/005.
- [71] D. N. Maksimov, A. F. Sadreev, A. A. Lyapina, A. S. Pilipchuk, Coupled mode theory for acoustic resonators, Wave Motion 56 (2015) 52–66. doi:10.1016/j.wavemoti.2015.02.003.

- [72] K. Pichugin, H. Schanz, P. Šeba, Effective coupling for open billiards, Physical Review E 64 (5) (2001) 056227. doi:10.1103/physreve.64.056227.
- [73] J. Okołowicz, M. Płoszajczak, I. Rotter, Dynamics of quantum systems embedded in a continuum, Physics Reports 374 (4-5) (2003) 271–383. doi:10.1016/s0370-1573(02)00366-6.
- [74] C. Mahaux, H. Weidenmueller, Shell-model approach to nuclear reactions, North-Holland,, Amsterdam,, 1969.
- [75] H.-J. Stöckmann, Quantum Chaos: An Introduction, Cambridge University Press, Cambridge, U.K., 1999.
- [76] Y. Alhassid, The statistical theory of quantum dots, Reviews of Modern Physics 72 (2000) 895.
- [77] H.-J. Stöckmann, E. Persson, Y.-H. Kim, M. Barth, U. Kuhl, I. Rotter, Effective hamiltonian for a microwave billiard with attached waveguide, Physical Review E 65 (6) (2002) 066211. doi:10.1103/physreve.65.066211.
- [78] G. Akguc, T. Seligman, Efficient method for scattering problems in open billiards: Theory and applications, Phys. Rev. B 74 (2006) 245317. doi:10.1103/physrevb.74.245317.
- [79] N. Auerbach, V. Zelevinsky, Super-radiant dynamics, doorways and resonances in nuclei and other open mesoscopic systems, Rep. Progr. Phys. 74 (2011) 106301. doi:10.1088/0034-4885/74/10/106301.
- [80] S. Datta, Electronic transport in mesoscopic systems, Cambridge University Press, U.K., 1995.
- [81] A. F. Sadreev, Feshbach projection formalism for transmission through a time-periodic potential, Phys. Rev. E 86 (5) (2012) 056211. doi:10.1103/physreve.86.056211. URL http://dx.doi.org/10.1103/PhysRevE.86.056211
- [82] N. Hatano, Equivalence of the effective hamiltonian approach and the siegert boundary condition for resonant states, Fortschr. Phys. 61 (2-3) (2012) 238–249. doi:10.1002/prop.201200064.
- [83] N. Hatano, G. Ordonez, Time-reversal symmetric resolution of unity without background integrals in open quantum systems, Journal of Mathematical Physics 55 (12) (2014) 122106. doi:10.1063/1.4904200.
- [84] E. Bulgakov, A. Sadreev, Symmetry breaking in a t-shaped photonic waveguide coupled with two identical nonlinear cavities, Phys. Rev. B 84 (2011). doi:10.1103/physrevb.84.155304.
- [85] A. A. Lyapina, D. N. Maksimov, A. S. Pilipchuk, A. F. Sadreev, Bound states in the continuum in open acoustic resonators, Journal of Fluid Mechanics 780 (2015) 370–387. doi:10.1017/jfm.2015.480.
- [86] N. Moiseyev, Quantum theory of resonances: calculating energies, widths and cross-sections by complex scaling, Physics Rep. 302 (5-6) (1998) 212–293. doi:10.1016/s0370-1573(98)00002-7.
- [87] E. N. Bulgakov, I. Rotter, A. F. Sadreev, Comment on "bound-state eigenenergy outside and inside the continuum for unstable multilevel systems", Phys. Rev. A 75 (jun 2007). doi:10.1103/physreva.75.067401.
- [88] R. Kikkawa, M. Nishida, Y. Kadoya, Polarization-based branch selection of bound states in the continuum in dielectric waveguide modes anti-crossed by a metal grating, New Journal of Physics 21 (11) (2019) 113020. doi:10.1088/1367-2630/ab4f54.
- [89] P. Markoš, C. Soukoulis, Wave Propagation: From Electrons to Photonic Crystals and Left-Handed Materials Princeton Univ, Press, 2008.
- [90] P. W. Anderson, Absence of diffusion in certain random lattices, Phys. Rev. 109 (1958) 1492-1505. doi:10.1103/physrev.109.1492.
- [91] Y. Aharonov, D. Bohm, Significance of electromagnetic potentials in the quantum theory, Phys. Rev. 115 (1959) 485-491. doi:10.1103/physrev.115.485.
- [92] E. N. Bulgakov, K. N. Pichugin, A. F. Sadreev, I. Rotter, Bound states in the continuum in open aharonov-bohm rings, JETP Lett. 84 (2006) 430–435. doi:10.1134/s0021364006200057.
- [93] J.-B. Xia, Quantum waveguide theory for mesoscopic structures, Phys. Rev. B 45 (7) (1992) 3593–3599. doi:10.1103/physrevb.45.3593.
- [94] V. I. Smirnov, A Course of Higher Mathematics, Vol. 3, Pergamon Press, Oxford, Oxford, 1964.
- [95] C. Texier, Scattering theory on graphs: II. the friedel sum rule, J. Phys. A: Math. and Gen. 35 (15) (2002) 3389–3407. doi:10.1088/0305-4470/35/15/303.
- [96] C. Texier, M. Buttiker, Local friedel sum rule on graphs, Phys. Rev. B 67 (24) (2003). doi:10.1103/physrevb.67.245410.
- [97] P. S. Pankin, B.-R. Wu, J.-H. Yang, K.-P. Chen, I. V. Timofeev, A. F. Sadreev, One-dimensional photonic bound states in the continuum, Communications Physics 3 (2020) 1–8. doi:10.1038/s42005-020-0353-z.
- [98] J. D. Jackson, Classical Electrodynamics, John Wiley and Sons, Inc.,, New York, 1962.
- [99] A.-S. Bonnet-Bendhia, F. Starling, Guided waves by electromagnetic gratings and non-uniqueness examples for the diffraction problem, Mathematical Methods in the Applied Sciences 17 (1994) 305–338. doi:10.1002/mma.1670170502.
- [100] S. Rotter, F. Libisch, J. Burgdorfer, U. Kuhl, H.-J. Stockmann, Tunable fano resonances in transport through microwave billiards, Phys. Rev. E 69 (2004). doi:10.1103/physreve.69.046208.
- [101] A. Lyapina, A. Pilipchuk, A. Sadreev, Bound states with orbital angular momentum in the continuum of cylindrical non axisymmetric waveguide, Annals of Physics 396 (2018) 56–70. doi:10.1016/j.aop.2018.05.020.
- [102] A. Lyapina, A. Pilipchuk, A. Sadreev, Trapped modes in a non-axisymmetric cylindrical waveguide, J. Sound and Vibr. 421 (2018) 48–60. doi:10.1016/j.jsv.2018.01.056.
- [103] F. Remacle, M. Munster, V. Pavlov-Verevkin, M. Desouter-Lecomte, Trapping in competitive decay of degenerate states, Phys. Lett. A 145 (1990) 265–268. doi:10.1016/0375-9601(90)90361-q.
- [104] Bo Zhen, Chia Wei Hsu, Ling Lu, A. D. Stone, M. Soljačić, Strong resonances on periodic arrays of cylinders and optical bistability with weak incident waves, Phys. Rev. Lett 113 (2014) 257401.
- [105] E. Bulgakov, A. Sadreev, Spin polarized bound states in the continuum in open aharonov–bohm rings with the rashba spin–orbit interaction, J. Phys.: Cond. Matt. 28 (2016) 265301. doi:10.1088/0953-8984/28/26/265301.
- [106] S. Dai, L. Liu, D. Han, J. Zi, From topologically protected coherent perfect reflection to bound states in the continuum, Phys. Rev. B 98 (2018) 081405. doi:10.1103/physrevb.98.081405.
- [107] A. Sadreev, A. Pilipchuk, A. Lyapina, Tuning of fano resonances by rotation of continuum: Wave faucet, Europhys. Lett. 117 (2017) 50011. doi:10.1209/0295-5075/117/50011.
- [108] A. Sadreev, A. S. Pilipchuk, A. A. Pilipchuk, Tuning of fano resonance by waveguide rotation, in: Springer Series in Optical Sciences,

- Springer International Publishing, 2018, p. 497. doi:10.1007/978-3-319-99731-5.
- [109] M. Born, E. Wolf, Principles of Optics: Electromagnetic Theory of Propagation, Interference and Diffraction of Light, Cambridge University Press, 1999.
- [110] A. E. Miroshnichenko, Y. S. Kivshar, Engineering fano resonances in discrete arrays, Physical Review E 72 (2005) 056611. doi:10.1103/physreve.72.056611.
- [111] Z. Wang, S. Fan, Compact all-pass filters in photonic crystals as the building block for high-capacity optical delay lines, Phys. Rev. E 68 (2003) 066616. doi:10.1103/physreve.68.066616.
- [112] L.-L. Lin, Z.-Y. Li, B. Lin, Engineering waveguide-cavity resonant side coupling in a dynamically tunable ultracompact photonic crystal filter, Physical Review B 72 (16) (2005). doi:10.1103/physrevb.72.165330.
- [113] K. Pichugin, A. Sadreev, Self-induced light trapping in nonlinear fabry-perot resonators, Physics Letters A 380 (2016) 3570-3574. doi:10.1016/j.physleta.2016.08.032.
- [114] H.-W. Lee, Generic transmission zeros and in-phase resonances in time-reversal symmetric single channel transport, Physical Review Letters 82 (1999) 2358–2361.